

Article

Air-Outlet and Step-Number Effects on a Step-like Plenum Battery's Thermal Management System

Olanrewaju M. Oyewola ^{1,*}, Emmanuel T. Idowu ¹, Morakinyo J. Labiran ¹ , Michael C. Hatfield ² and Mebougna L. Drabo ³

¹ Department of Mechanical Engineering, University of Alaska Fairbanks, Fairbanks, AK 99775, USA; etidowu@alaska.edu (E.T.I.); mlabiran@alaska.edu (M.J.L.)

² Department of Electrical and Computer Engineering, University of Alaska Fairbanks, Fairbanks, AK 99775, USA; mchatfield@alaska.edu

³ Department of Mechanical & Civil Engineering and Construction Management, Alabama A&M University, Huntsville, AL 35811, USA; mebougna.drabo@aamu.edu

* Correspondence: ooyewola@alaska.edu or oooyewola001@gmail.com

Abstract: Optimizing the control of the battery temperature (T_b), while minimizing the pressure drop (ΔP) in air-cooled thermal management systems (TMSs), is an indispensable target for researchers. The Z-type battery thermal management system's (BTMS's) structure is one of the widely investigated air-cooled TMSs. Several designs of air-cooled BTMSs are often associated with the drawback of a rise in ΔP , consequently resulting in an increase in pumping costs. In this study, the investigation of a Step-like plenum design was extended by exploring one and two outlets to determine possible decreases in the maximum battery temperature (T_{max}), maximum battery temperature difference (ΔT_{max}), and pressure drop (ΔP). The computational fluid dynamics (CFD) method was employed to predict the performances of different designs. The designs combine Step-like plenum and two outlets, with the outlets located at different points on the BTMS. The results from the study revealed that using a one-outlet design, combined with a Step-like plenum design, reduced T_{max} by 3.52 K when compared with that of the original Z-type system. For another design with two outlets and the same Step-like plenum design, a reduction in T_{max} by 3.45 K was achieved. For ΔT_{max} , the use of a two-outlet design and a Step-like plenum design achieved a reduction of 6.34 K. Considering the ΔP performance, the best- and poorest-performing designs with two outlets reduced ΔP by 5.91 Pa and 3.66 Pa, respectively, when compared with that of the original Z-type design. The performances of the designs in this study clearly show the potential of two-outlet designs in reducing ΔP in systems. This study, therefore, concludes that the operational cost of the Step-like plenum Z-type BTMS can be reduced through the careful positioning of the two-outlet section, which will promote the design and development of current and future electric vehicle (EV) technologies.

Keywords: air outlet; step number; pressure drop; temperature; BTMS



Academic Editors: Xianglin Li, Chuanbo Yang and Prahit Dubey

Received: 26 January 2025

Revised: 14 February 2025

Accepted: 19 February 2025

Published: 21 February 2025

Citation: Oyewola, O.M.; Idowu, E.T.; Labiran, M.J.; Hatfield, M.C.; Drabo, M.L. Air-Outlet and Step-Number Effects on a Step-like Plenum Battery's Thermal Management System. *Batteries* **2025**, *11*, 87. <https://doi.org/10.3390/batteries11030087>

Copyright: © 2025 by the authors. Licensee MDPI, Basel, Switzerland. This article is an open access article distributed under the terms and conditions of the Creative Commons Attribution (CC BY) license (<https://creativecommons.org/licenses/by/4.0/>).

1. Introduction

The performance enhancement of battery thermal management systems (BTMSs) has been a vital research focus in recent times because of their roles in advancing the design and development of novel highly efficient electric vehicles (EVs). Over the years, EVs have proven to be reliable in the bid to minimize environmental pollution and fossil fuel consumption [1] because of the choice of batteries as an energy source as an alternative

to conventional fossil fuels. Different types of batteries have been used to power EVs; however, the most common type is the lithium-ion battery. The power consumption, mileage, and cost of electric vehicles generally depend on the health and capacity of batteries [2]. Interestingly, despite their wide acceptance, lithium-ion batteries generate too much heat during charging and discharging, which poses severe threats to the health and service life of the batteries. In order to overcome this challenge, novel BTMSs that are highly efficient and effective must be developed. Generally, BTMSs are required to maintain the working temperature of battery packs between 25 °C and 40 °C, while the maximum temperature difference (ΔT_{max}) between any two batteries in a pack remains below 5 °C [3,4]. This is necessary because a ΔT_{max} value higher than the recommended value and temperatures outside the recommended range will negatively impact the performance of batteries [5]. Several cooling methods for BTMSs have been developed over the years and can be categorized as passive and active cooling methods. For active cooling, batteries are cooled by passing air across the batteries [6,7], by the direct contact of liquid on the batteries, by passing the liquid through cooling plates or mini channels [8,9], or by placing heat pipes between and around batteries [10,11]. Passive cooling utilizes phase-change materials (PCMs), which will be in direct contact with batteries to maintain the batteries' operational temperature [12,13]. The combination of two methods has also been explored, such as passive/passive, active/active, or passive/active methods [14–16]. Despite the progress recorded in the design of BTMSs, the air-cooling BTMS still remains one of the most preferred choices because of its numerous benefits of design affordability, simplicity, stability, light weight, and longevity [17]. It has been employed by many companies, such as Nissan, Toyota, Volkswagen, and Chevrolet [17,18].

The research on the air-cooling technique is being explored, with new designs supplementing the air-cooling techniques by adding other enhancement techniques, to form hybrid thermal management systems (HTMSs). Focusing HTMSs, Mo et al. [1] combined phase-change materials (PCMs) and air-cooling techniques for managing the performance of batteries under all climate conditions. In a study by Qin et al. [19], PCMs and air-cooling techniques were integrated together to form a hybrid BTMS, which was investigated experimentally and numerically. Behi et al. [20] proposed a novel concept that combines heat pipes and air-cooling for managing battery temperatures in electric vehicles. Zhang et al. [21] carried out a performance analysis of another hybrid BTMS, which combines PCMs and air-cooling, by leveraging the potential of machine-learning algorithms to optimize the choice of the operational and structural parameters of the design. Zhou et al. [22] utilized liquid cooling while designing the channel for the liquid flow in the form of steps. A new concept has also emerged for PCMs, as reported by Song et al. [23], where a dual-layer PCM was designed, while air provided additional cooling. A recent concept proposed by Zhu et al. [24] combined two different outlet positions employed in the Z-type BTMS. The PCM-based hybrid design has been further investigated using nano-PCM, fins, and metal foam [25,26]. The modification of the structural orientations of battery packs to optimize their performance has also been widely employed. Argade and De [27] optimized the design of the Z-type BTMS by adopting a tapered air inlet and secondary vents. Oyewola and Idowu [28] investigated the waved and straight structures of the divergence plenum of the Z-type BTMS to alter the flow of the air to improve the thermal uniformity. Suo et al. [29] also investigated the effects of different plenum shapes, such as slanted, convex, concave, and stepped, and different plenum positions on the heat dissipation performances of batteries. Chen et al. [30] explored a control strategy based on the temperature difference among batteries for a J-type-structured BTMS. Alzwayi and Paul [31] considered the control of flow patterns while introducing vertical and spiral fins to enhance the cooling performance of the system. The installation of baffles, spoilers, and fins along the airflow

path has been widely adopted. For instance, Qin et al. [32] carried out experimental and numerical simulation studies for a design with a combination of internal fin structures and air cooling to enhance the thermal performance of a system. Wang et al. [33] installed spoilers along the airflow path to enhance the thermal performance of the Z-type BTMS. Wang et al. [34] introduced parallel plates to the airflow of the same Z-type BTMS to enhance the performance of the system. Oyewola et al. [35] investigated the use of straight and inclined baffles in enhancing the performance of the Z-type BTMS. Alzwayi and Paul [36] examined the heat transfer enhancement of batteries using vertical and spiral cooling fins. Each of these studies provides distinct performances and demonstrates huge potential in enhancing the performance of Z-type BTMSs.

The findings from a few of the aforementioned studies are further presented to demonstrate how they impact the thermal performances of batteries. A study by Wang et al. [34] added parallel plates to the Z-type BTMS to enhance its performance. It was revealed that this technique reduced T_{max} and ΔT_{max} by 3.37 K (6.17%) and 5.5 K (71.9%), respectively, in comparison with those of the original Z-type design. In a study by Oyewola et al. [35], where straight and inclined baffles were installed to understand how they influence the performance of the system, the results showed that the baffle thickness can either decrease or increase the T_{max} values of the batteries, while inclined baffles generally produce better T_{max} and ΔP performances. In a study by Alzwayi and Paul [36], the heat transfer enhancement in a Z-type BTMS with cylindrical lithium-ion batteries having vertical and spiral fins installed on them was investigated. It was observed that spiral fins reduced the battery temperature by 3.2% when compared with longitudinal fins, which also resulted in a 65.6% reduction in the amount of material used. Other studies that explore the hybrid approach have also reported enhancements in performance. For instance, Moaveni et al. [26] investigated passive and hybrid BTMSs by employing fins, nano-PCMs, and metal foam, which served as flow control mechanisms. From the study, using 9% nanoparticles and four fins in the hybrid system, T_{max} reduced by 5.18 K and 10.36 K, when compared with that of the system without fins and nanoparticles, respectively. Song et al. [23] considered a hybrid BTMS having a double-layer PCM and air-cooling techniques. The T_{max} value of the hybrid BTMS achieved a reduction of 21.5% in comparison with that of the PCM BTMS at an ambient temperature of 40 °C. The aforementioned studies reported improvements in the thermal performance of the BTMS, with most of the techniques requiring the addition of materials, which, consequently, implies an increase in the overall weight of the system. This is not favorable in applications where weight reduction is crucial to achieve the optimal operation. Hence, more studies have been carried out to improve thermal performance without necessarily adding more materials. One such approach can be seen in a study by Oyewola et al. [28], where different wave-like and straight configurations were investigated. The study reported that ΔT_{max} and T_{max} reduced by 8 K and 4.61 K, respectively, using a wave-inclined plenum configuration. Targeting improvement in thermal performance without adding materials, Argade and De [27] created outlet vents on the convergence plenum while further redesigning the divergence plenum to have an inclined configuration. The study revealed that T_{max} and ΔT_{max} were reduced by 2.18% and 72.84% when compared to those of the system without vents.

From the literature presented in this study, it is evident that Z-type BTMSs have been extensively investigated through different structural modifications. One of these designs that has shown huge thermal enhancement potential is the Step-like plenum BTMS, with a significant reduction in T_{max} . A lot of investigations have also been conducted on the Z-type BTMS with a Step-like plenum design to gain detailed insight into the performance of the design. Zhou et al. [22] proposed stepped channels to achieve a lightweight design, using liquid as a cooling fluid. Zhu et al. [24] combined the Step-

like design with two outlet positions. Oyewola et al. [37] also investigated the Step-like design, focusing on four different numbers of steps, with each design having the same step height. In order to better understand the Step-like design, Oyewola et al. [38] investigated each number of steps with variable step heights. A further study by Oyewola et al. [39] leveraged machine learning's benefits to investigate additional numbers of steps and various inlet air velocities and temperatures. Each of these studies demonstrates different performances in terms of T_{max} , ΔT_{max} , and ΔP . By installing steps on the divergent plenum and changing the positions of the outlets, the performances of the designs varied. However, increases in the pressure drop were recorded for all the Step-like plenum designs. This work differs from the previous works by investigating the performance of Step-like plenum BTMSs through the introduction of two outlets, positioned at different locations on the convergent plenum, with the aim of maintaining a reduction in T_{max} while reasonably reducing ΔP . Considering the potential of increasing the number of steps while adopting and repositioning two outlet channels, more investigations can be carried out for the Step-like plenum configuration. In view of these, the current study explored additional possibilities not covered by Oyewola et al. [37] and Oyewola et al. [39] by investigating seven different numbers of steps, combined with one or two outlets, placed at different flow pattern positions. The numerical simulation method was employed to investigate different structural designs, thereby proposing the best structure in terms of reductions in T_{max} , ΔT_{max} , and ΔP . It should be noted that the performances of these designs will be presented based on each of the aforementioned parameters and not based on a combined effect of the three parameters. A future study is underway to optimize the designs and select the performance metric that balances the tradeoffs between the parameters.

2. Simulation Method

A computational fluid dynamics (CFD) approach was adopted, with the reference Z-type BTMS as the primary design. From the literature, it can be seen that several modifications of Z-type BTMs have been developed and investigated, with the aim of minimizing heat accumulation and pressure loss during cooling. The studies have revealed that parameters such as the maximum temperature (T_{max}), maximum temperature difference (ΔT_{max}), and pressure drop (ΔP) are significant in evaluating the performance of the system [30,31,40]. Air-cooled BTMSs aim to prevent excess temperature accumulation through reductions in T_{max} , promote thermal homogeneity through reductions in ΔT_{max} , and minimize pumping costs through reductions in ΔP . These are general performance metrics extensively reported in air-cooled battery thermal management system studies. Furthermore, a reduction in ΔT_{max} indicates improvement in thermal homogeneity (uniform temperature distribution) among the batteries in a pack. Improvement in thermal homogeneity decreases the possibility of irregular heating, which could cause the overheating of a battery at the expense of the other batteries in the same pack, maintaining significantly lower temperatures. Such overheating affects the lifespan of batteries and could lead to explosions [5,37,40]. The CFD tool used for this study is the well-known ANSYS software 2024 R1 package. This software was used for developing physical geometries, meshing and independence tests, and computing the appropriate governing equations to predict the airflow and temperature profiles of BTMSs.

2.1. Physical Geometries

2.1.1. Z-Type Geometry

The widely investigated Z-type BTMS (denoted as Z-1) structure was considered in this study because of its simplistic shape, configuration, and arrangement of batteries. An experimental study has been carried out for this structure to establish and evaluate its

reliability for real-life applications. Additionally, 3D and 2D geometries of the BTMS have been investigated, with the results showing very good comparative performances [40]. A numerical simulation by Chen et al. [40] compared the performances of conventional Z-type BTMSs using 2D and 3D geometries. The results showed a negligible difference between the two geometries, with estimated average errors of 1% and 0.1% for the airflow and temperature of the batteries, respectively. Moreso, simulations with 2D geometries were faster than those with 3D geometries. Based on this assertion, 2D geometries were considered for all the numerical simulations in this study. Figure 1a–d shows a 2D Z-type BTMS, a 2D battery, a 3D Z-type BTMS, and a 3D battery, respectively. The BTMS consists of an inlet section and an outlet section for passing in air and rejecting air, respectively, while eight batteries in a series arrangement are cooled down. The air passes through cooling channels (CCs) during the cooling process. A cooling channel has fixed length (CC_l) at 3 mm, while the velocity (V_i) and temperature (T_i) of the air at the inlet are taken as 3 m/s and 299.15 K, respectively, with a heat power of 11.8 W. The heat generation rate of the battery can be estimated using Equation (1), for the 5-current constant discharge rate of the battery (12 Ah LiFePO₄) estimated at 69,370 W/m³ [40–42]. The properties of the battery and air are presented in Table 1 [34,37]. The description of the original Z-type BTMS is presented in Table 2.

$$Q_b = \left(I^2 R_b - IT_b \frac{du}{dT} \right) / V_b \quad (1)$$

$$R_b = 0.00705 - 0.01853 \times SOC + 0.05894 \times SOC^2 - 0.09151 \times SOC^3 + 0.06579 \times SOC^4 - 0.01707 \times SOC^5 \quad (2)$$

where I is the discharge current, R_b is the battery's equivalent resistance, T_b is the battery temperature, V_b is the volume of the battery, and $\frac{du}{dT} = -0.22$ mV/K is a coefficient obtained from electrochemical–calorimetric techniques.

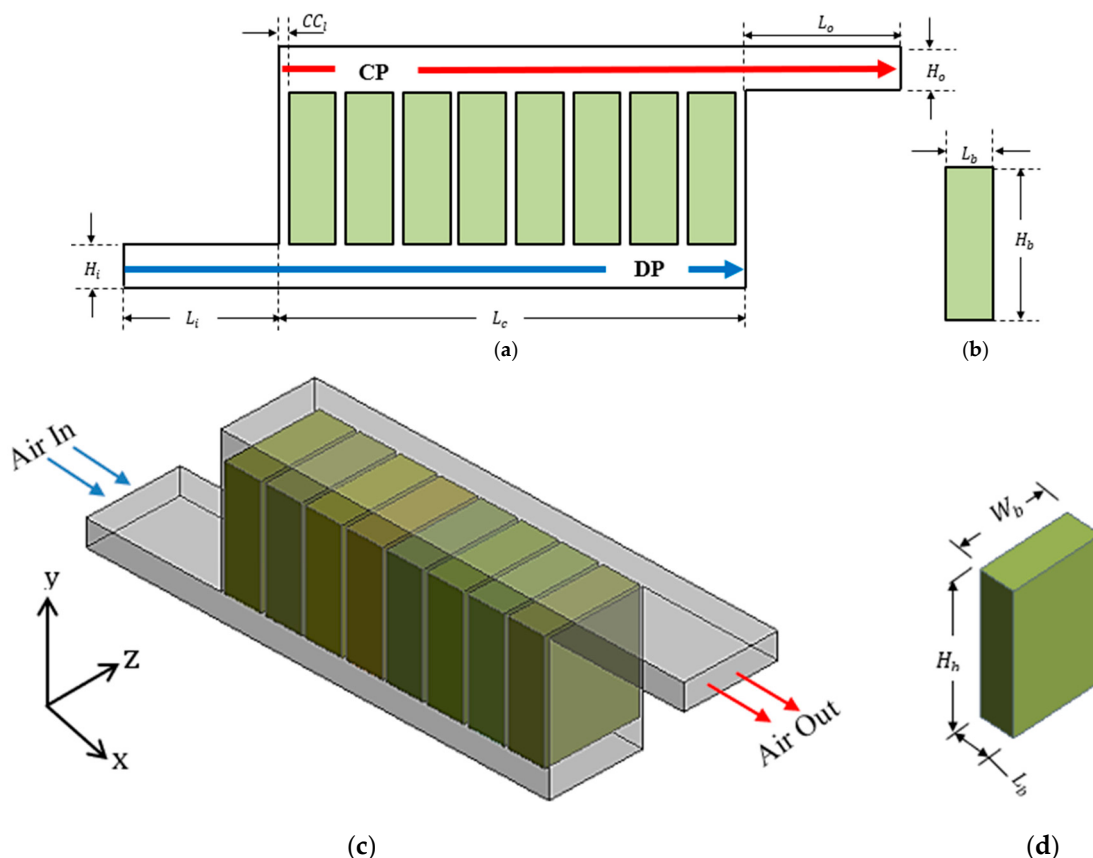


Figure 1. Z-type (a) 2D BTMS, (b) 2D battery, (c) 3D BTMS, and (d) 3D battery [34,40].

Table 1. Properties of the air and battery [34,37].

Property	Battery	Air	Unit
Specific heat (c_p)	1337	1005	J/kgK
Density (ρ)	1542.9	1.165	kg/m ³
Dynamic viscosity (μ)	-	1.86×10^{-5}	kg/ms
Thermal conductivity (k)	1.05 (x); 21.1 (y); 21.1 (z)	0.0267	W/mK

Table 2. Geometric and flow properties of the Z-type and Step-like BTMSs [34,37].

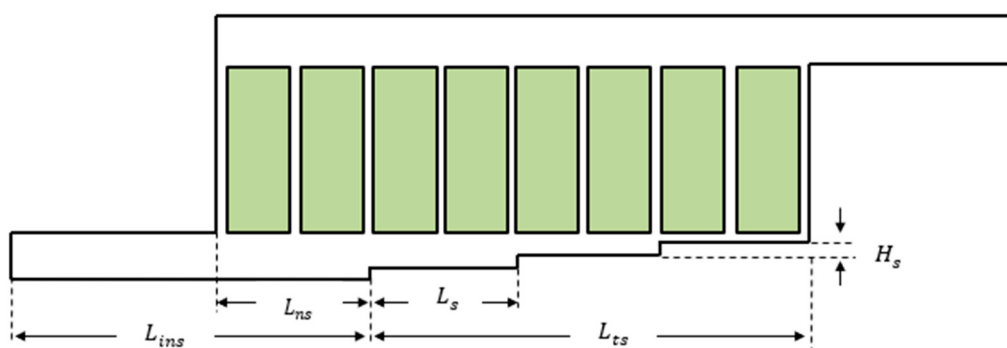
Description	Symbol	Value (mm)
Length of the cooling channel	CC_l	3
Length of the inlet/outlet section	L_i/L_o	100
Length of the cooling section	L_c	243
Length of the battery	L_b	27
Height of the inlet/outlet section	H_i/H_o	20
Height of the battery	H_b	90
Width of the inlet/outlet section	W_i/W_o	70
Width of the battery	W_b	70
Convergence plenum	CP	343
Divergence plenum	DP	343

2.1.2. Step-Like Plenum Geometry

The Step-like plenum geometry (Z-2) considered in this study was initially proposed by Oyewola et al. [37]. This geometry has further been studied by exploring some modifications to the step characteristics, such as increasing the number of steps (N_s) and varying the step height (H_s) [38,39]. Figure 2 shows a 2D schematic view of the Step-like plenum geometry and its characteristics, viz., the step number (N_s), height of the step (H_s), and length of the step (L_s). In the initial design by Oyewola et al. [37], it was reported that the step number is obtained by setting the step length to hover under each battery and CC along the length of the cooling section (L_c). Also, in order to ensure the heights of the steps are identical, the height must be an integer. The height of a step is calculated using Equation (3), while its corresponding length is calculated using Equation (4). The N_s values designed are 1, 3, 4, 7, 9, 15, and 19, denoted as Z-2-1, Z-2-3, Z-2-4, Z-2-7, Z-2-9, Z-2-15, and Z-2-19, respectively.

$$H_s = \frac{H_i}{N_s + 1} \quad (3)$$

$$L_s = \frac{L_c - CC_l}{N_s + 1} \quad (4)$$

**Figure 2.** Two-dimensional schematic view of the Step-like plenum geometry.

2.1.3. One-Outlet Geometry

A one-outlet geometry Z-type design simply refers to a design with only one outlet section. In order to enhance the BTMSs' performances, some researchers have explored novel strategies to offset heat by introducing an extra outlet or creating vents [27,43]. For the one-outlet design, the location of the outlet section was varied, and four different locations, which have been investigated, were selected, whereby the cooling air in the outlet direction becomes perpendicular, parallel, and/or opposite to the cooling air's direction in the inlet section. These outlet directions have been investigated by researchers [17,31,44] with smooth and modified divergence plenums. The selected four outlet section directions in this study are shown in Figure 3, while their descriptions are presented in Table 3. In addition, each one-outlet geometry is installed with a Step-like design for each of the seven step numbers (1, 3, 4, 7, 9, 15, and 19).

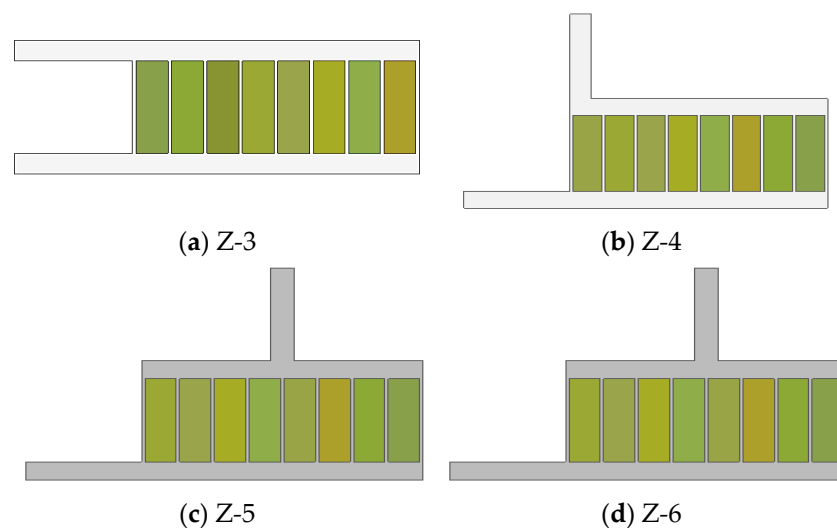


Figure 3. Schematics of one-outlet flow pattern designs.

Table 3. Descriptions of the one-outlet designs [28].

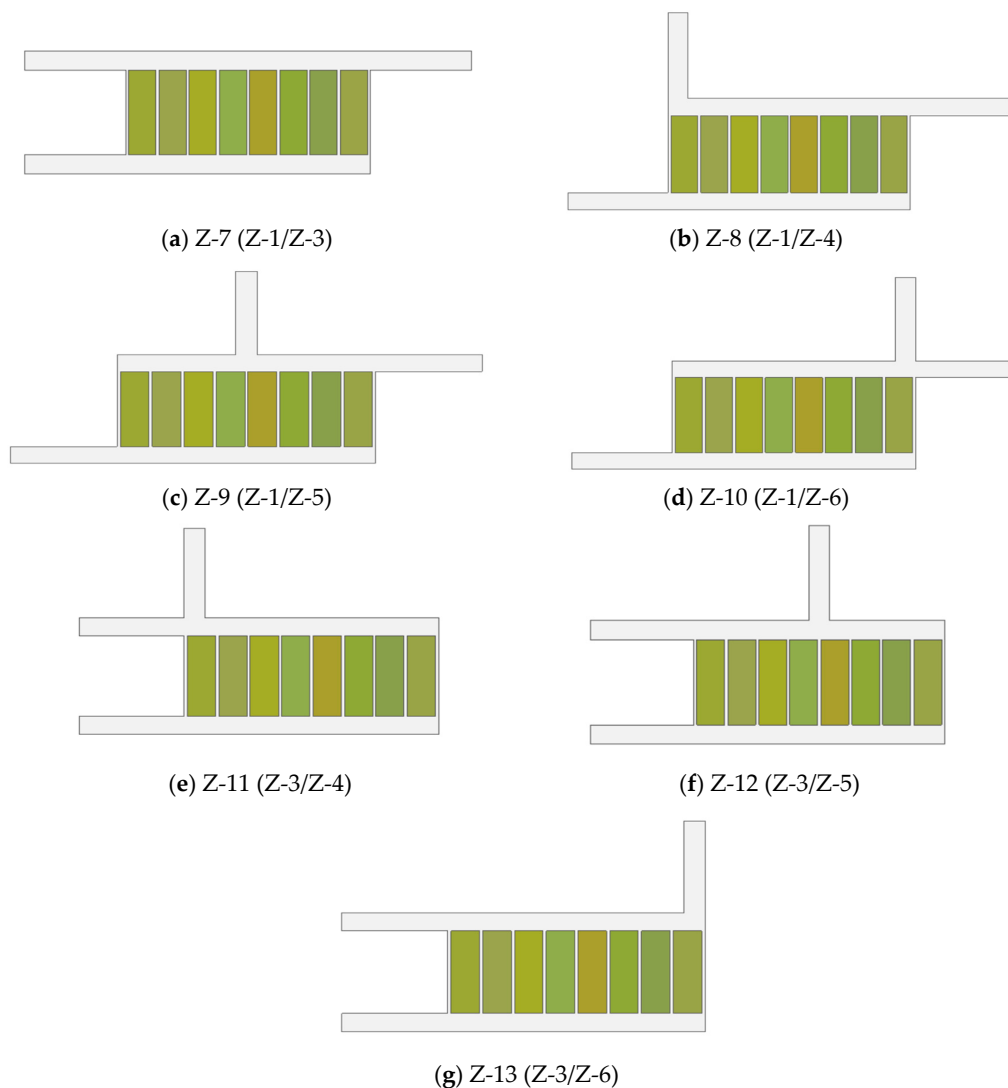
BTMS	Details
Z-3	Both the inlet and outlet sections are positioned perpendicular to CC on the same side.
Z-4	The outlet section is at the extreme edge of the plenum, perpendicular and close to the inlet section.
Z-5	The outlet section is at the midpoint of the plenum and perpendicular to the inlet section.
Z-6	The outlet section is at the extreme edge of the plenum, perpendicular to and farthest from the inlet section.

2.1.4. Two-Outlet Geometry

The two-outlet geometry is an approach with two outlet sections, which has attracted attention in the enhancement of the BTMS performance. From previous studies, the position of one outlet has been investigated on almost the entire perimeter of the geometry. However, researchers in recent times have been exploring adding one more outlet, to have two outlets, while interchanging their positions. This method has been explored, and the results have shown that it provides improvement in thermal and hydraulic performances [24,31]. Leveraging the potential of this method, this study investigated introducing two outlets to the Step-like design for each of the seven step numbers (1, 3, 4, 7, 9, 15, and 19). Table 4 presents the descriptions of the two-outlet designs, while Figure 4a–g shows the 2D geometries of the designs.

Table 4. Descriptions of the two-outlet geometries.

BTMS	Combination	Details
Z-7	Z-1/Z-3	This design basically has two outlets by adopting and combining the Z-1 and Z-3 outlet positions.
Z-8	Z-1/Z-4	Similar to the Z-7 design, this design adopts and combines the Z-1 and Z-4 outlet positions.
Z-9	Z-1/Z-5	Similarly, this design adopts and combines the Z-1 and Z-5 outlet positions.
Z-10	Z-1/Z-6	Similarly, this design adopts and combines the Z-1 and Z-6 outlet positions.
Z-11	Z-3/Z-4	This design adopts and combines the Z-3 and Z-4 outlet positions.
Z-12	Z-3/Z-5	Similarly, this design adopts and combines the Z-3 and Z-5 outlet positions.
Z-13	Z-3/Z-6	Similarly, this design adopts and combines the Z-3 and Z-6 outlet positions.

**Figure 4.** Schematics of two-outlet flow pattern geometric designs.

2.1.5. Combined-Strategy Geometries

The idea of combining different strategies to develop a new BTMS design is an interesting design concept with promising benefits, especially when seeking to enhance thermal performance without significant increases in the overall weights of the systems. In this category, each of the one-outlet and two-outlet geometries is combined with each of the seven Step-like plenum geometries. Figure 5a,b shows typical combined-strategy geometries with one outlet and two outlets, respectively, and four steps.

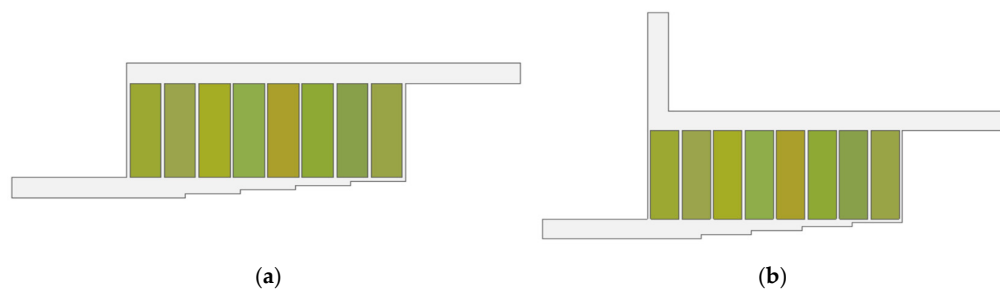


Figure 5. Selected combined-strategy geometries: (a) one outlet and (b) two outlets.

2.2. Numerical Simulations

In this study, the numerical simulations were based on the 2D geometries of the BTMSs. These simulations can be carried out for either steady-state or unsteady (transient)-state conditions, depending on the results targeted. When modeling Z-type BTMSs in a transient state, the thermal analysis will reach an equilibrium state (stable state) after a period of a continuous cooling time such that further increases in the cooling time will result in no change in the temperature of the batteries at a constant heat generation rate. This phenomenon was illustrated graphically during the transient cooling process of BTMSs in previous studies [33,45]. In cases where the numerical simulation results in the equilibrium state are of interest, a steady-state simulations is employed because a transient simulations takes a longer time to complete. An experimental study by Chen et al. [40] considered transient thermal analysis for both experimental and numerical simulation studies. Similar geometric and operational conditions utilized by Chen et al. [40] were successfully modeled in the steady state by Wang et al. [34] and Oyewola et al. [35]. Hence, all the solutions in this study were set in the steady state to minimize the computation time and cost. This study also employed governing equations, found in most commercial CFD tools, which have been adopted in modeling Z-type BTMSs [35,40], such as the continuity Equation (5) and the momentum Equation (6), for solving the flow problem, and the energy conservation Equation (7), for solving the thermal problem.

$$\nabla \cdot \vec{v} = 0 \quad (5)$$

$$\rho_a \frac{d\vec{v}}{dt} = -\nabla p + \mu_a \nabla^2 \vec{v} \quad (6)$$

$$\rho_a c_{pa} \frac{\partial T_a}{\partial t} + \nabla \cdot (\rho_a c_{pa} \vec{v} T_a) = \nabla \cdot (k_a \nabla T_a) \quad (7)$$

The Reynolds number, Re , is expressed using the equation:

$$Re = \frac{\rho_a V_i D_h}{\mu_a} \quad (8)$$

The hydraulic diameter is expressed using the equation:

$$D_h = \frac{2W_i H_i}{W_i + H_i} \quad (9)$$

The Reynolds number, Re , expressed using Equation (8), was estimated when the air's inlet velocity, V_i , was 3 m/s, which results in $Re = 5825$. Because the minimum estimated Re is greater than 3000, the flow is considered to be turbulent. Hence, the turbulence model (a standard $k - \epsilon$ model) was selected, expressed as Equations (10) and (11), for the turbulent kinetic energy and kinetic energy dissipation, respectively, while employing an enhanced wall treatment [35,40].

Turbulent kinetic energy equation, k :

$$\frac{\partial}{\partial t}(\rho k) + \frac{\partial}{\partial x_i}(\rho k u_i) = \frac{\partial}{\partial x_j} \left[\left(\mu + \frac{\mu_t}{\sigma_k} \right) \frac{\partial k}{\partial x_j} \right] + G_k + G_b - \rho \varepsilon - Y_M + S_k \quad (10)$$

Turbulent energy dissipation equation, ε :

$$\frac{\partial}{\partial t}(\rho \varepsilon) + \frac{\partial}{\partial x_i}(\rho \varepsilon u_i) = \frac{\partial}{\partial x_j} \left[\left(\mu + \frac{\mu_t}{\sigma_\varepsilon} \right) \frac{\partial \varepsilon}{\partial x_j} \right] + C_{1\varepsilon} \frac{\varepsilon}{k} (G_k + C_{3\varepsilon} G_b) - C_{2\varepsilon} \rho \frac{\varepsilon^2}{k} + S_\varepsilon \quad (11)$$

The turbulent viscosity is given as follows:

$$\mu_t = \rho C_\mu \frac{k^2}{\varepsilon} \quad (12)$$

The values of the model constants used in Equations (10)–(12) are $C_{1\varepsilon} = 1.44$, $C_{2\varepsilon} = 1.92$, $C_\mu = 0.09$, $\sigma_k = 1.0$, and $\sigma_\varepsilon = 1.3$.

The SIMPLE algorithm was selected for solving the governing equations. Additionally, convective and diffusive terms were discretized using central differencing and second-order terms, respectively. Convergence iteration residuals were set at 10^{-7} and 10^{-8} for flow terms and energy terms, respectively. The solution generally considered the following assumptions [33,35]:

1. The properties of the batteries and air are constant;
2. The air inlet flow is stable and incompressible;
3. The effect of the radiation is negligible;
4. The inlet air's velocity and temperature are constant.

The battery energy conservation Equation (13) [40,42] is

$$\rho_b c_{pb} \frac{\partial T}{\partial t} = \nabla \cdot (k_b \nabla T) + Q_b \quad (13)$$

In this study, the BTMSs' performances were generally evaluated by comparing the average temperature of each battery in the pack. Previous studies on Z-type BTMSs have measured the maximum temperature of the second battery (T_2), denoted as " T_{max} ", while the minimum temperature was at the eighth battery (T_8), denoted as T_{min} [34,35,37,40]. The difference between T_{max} and T_{min} , also known as the maximum temperature difference of the batteries, ΔT_{max} , is expressed as in Equation (14).

The battery's maximum temperature difference is expressed as follows:

$$\Delta T_{max} = T_{max} - T_{min} \quad (14)$$

The pressure drops (ΔP) across the BTMSs were also estimated using Equation (15). It is the difference between the average pressures at the inlet and outlet(s).

$$\Delta P = P_i - P_o \quad (15)$$

The ΔP value of the BTMS is associated with the pumping power, which, consequently, may result in increasing the pumping cost.

2.3. Boundary Conditions

For the inlet section, the air velocity (3 m/s) and temperature (299.15 K) boundary conditions were initially assigned to be constant [34,37]. Additional solutions were carried

out at inlet velocities of 3.5 m/s and 4 m/s, while the other settings remained the same. In general, the following assumptions were considered for the simulations [34,35,37]:

1. The heat generation rate assigned to the battery's surface was constant;
2. The zero (0)-gauge outlet pressure condition was assigned;
3. On the battery walls and inner walls of the systems, the no-slip condition was assigned;
4. An adiabatic wall was assigned to the entire surrounding wall of the systems;
5. The surrounding temperature and pressure were constant;
6. The contacting surfaces were set as coupled.

2.4. Meshing and Independence Study

All the geometries considered in this study were meshed on the ANSYS meshing platform. When setting up the meshing, five inflation layers were assigned at the boundary walls of the batteries, air domain, and system, while a height of 0.1 mm was set for the first layer (y^+) [33,34,37].

The mesh size can be improved by varying the element size and selecting several other options available in ANSYS to produce coarse or fine meshes, which can significantly influence the result obtained. However, by taking into consideration the available computation resources and time availability, a mesh independence study was carried out. This ensures that the solution is accurate at the minimum computational time possible. This targets the minimum possible number of elements from a meshed design, which results will have a negligible difference when results with a high number of elements are used [33,34,37]. Meshes were compared for seven element sizes ranging from 0.00065 to 0.00035 at 0.00005 intervals, and the corresponding numbers of elements for these element sizes are 121,383; 140,625; 166,368; 198,584; 244,027; 308,204; and 400,154, respectively. The independence study performances are further presented graphically in Figure 6a,b. As the number of elements increases from 308,204 to 400,154, the variation in the parameters was negligible, with differences of 0.02 K, 0.01 K, 0.03 K, and 0 Pa for T_{max} , T_{min} , ΔT_{max} , and ΔP , respectively. Therefore, the mesh setup that produced a mesh size of 400,154 was used for simulating other models.

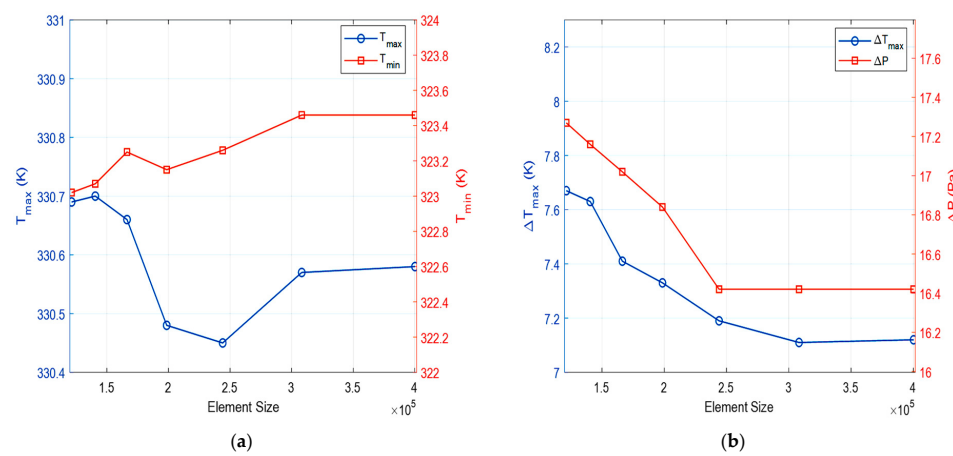


Figure 6. Mesh independence tests: (a) T_{max} and T_{min} and (b) ΔT_{max} and ΔP .

2.5. CFD Method Validation

The results obtained from the simulations were compared with the experimental results, which has also been performed in previous studies for the original Z-type BTMS [28,33,34,37], by comparing the simulation results with the experimental results of Chen et al. [40]. The primary parameters used for the comparison are the average battery temperatures measured for the air's inlet velocities of 3, 3.5, and 4 m/s. In this study, the

average battery temperatures were measured, which also show very good agreement with the experimental results of Chen et al. [40]. Figure 7a,b presents the comparison for the maximum (T_{max}) and minimum (T_{min}) values, which were also measured for the second and eighth batteries, respectively. Figure 8a–d illustrates the 2D physical geometry, selected mesh, temperature contour, and air-velocity contour of the reference Z-type BTMS. From the comparison, maximum differences of 1.6 K (0.5%) and 0.65 K (0.2%) were obtained for T_{max} and T_{min} , respectively. Zhang et al. [46], reported that differences of up to 2% can be considered as negligible. Interestingly, the estimated values obtained in this study are below 2%. Therefore, the CFD method is considered as acceptable.

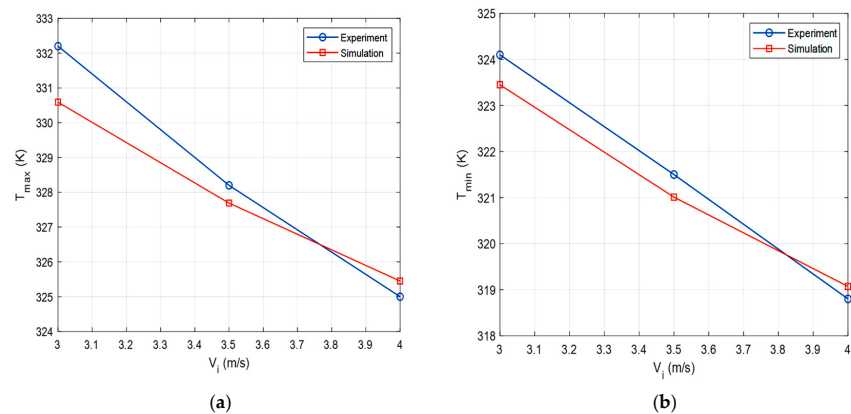


Figure 7. Comparison between experiments [40] and the CFD method (the current study) for (a) T_{max} and (b) T_{min} .

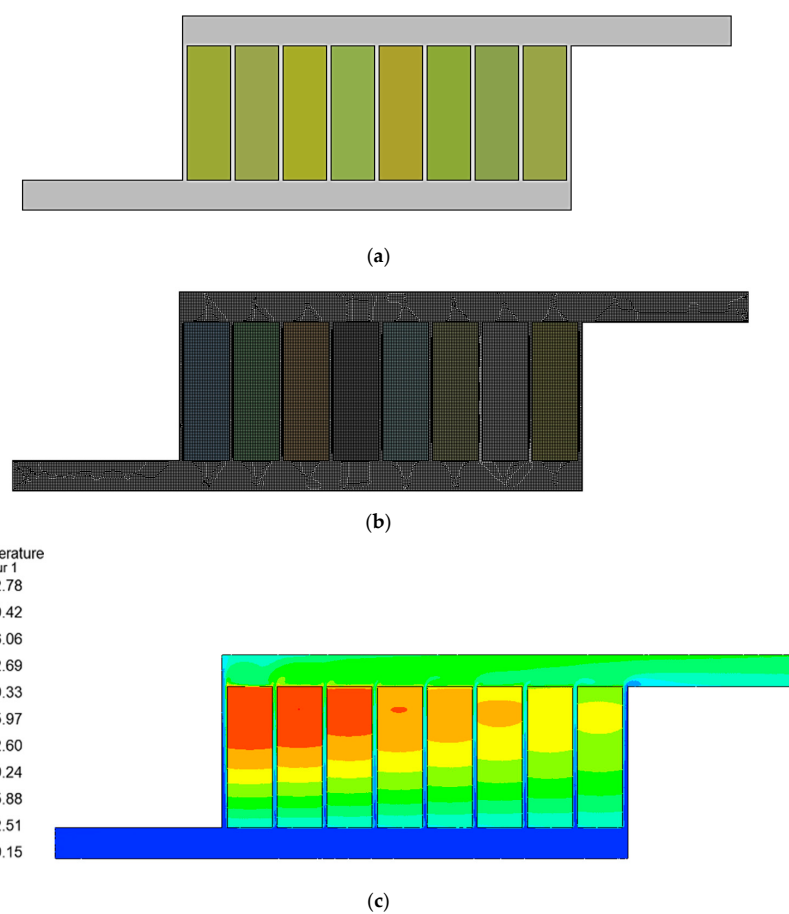


Figure 8. Cont.

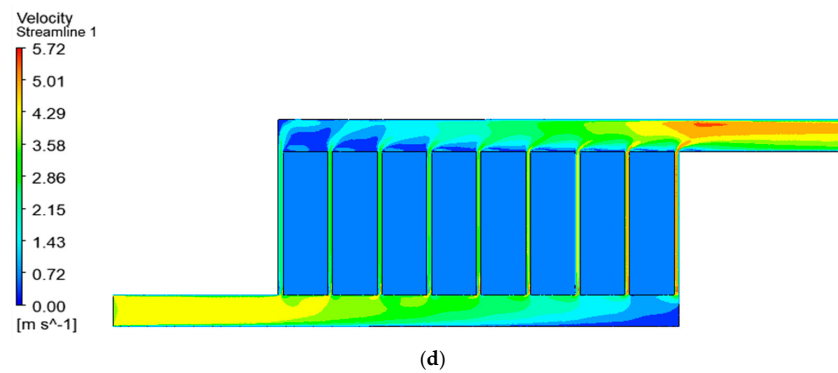


Figure 8. The reference Z-type BTMS's (a) 2D geometry, (b) selected mesh, (c) temperature contour, and (d) air-velocity contour.

3. Results and Discussion

In the development of BTMSs where air is the cooling fluid, it is important to minimize ΔP while maintaining the battery temperature or possibly minimizing the temperature. ΔP minimization is necessary because it corresponds to a reduction in the pumping cost. When focusing on minimizing the battery temperature, it is also important to ensure that it does not go below the recommended temperature. Hence, ΔT_{max} among the batteries is evaluated, which compares the thermal uniformity or homogeneity of the batteries in a BTMS. Based on these criteria, the designs will be compared based on T_{max} , ΔT_{max} , and ΔP . In general, a total of 95 geometries were developed, and the simulation results for each geometry were obtained at the air's inlet velocity and a temperature of 3 m/s and 299.15 K, respectively.

3.1. Evaluation of T_{max} Performances

One of the parameters considered for the thermal performances of BTMSs is T_{max} . In order to avoid the overheating of batteries and thermal runaway, it is imperative to design a BTMS such that T_{max} is minimized and maintained below the maximum recommended working temperature. In this section, the T_{max} values of the different designs are compared.

3.1.1. T_{max} Performances of Step-like Plenum, One-Outlet, and Two-Outlet Geometries

In this subsection, the T_{max} values for the Step-like plenum, one-outlet, and two-outlet designs are compared. Afterward, the best-performing designs (with the minimum T_{max} values) from each group are also compared. Figure 9a–c shows the variations in T_{max} for the Step-like plenum, one-outlet, and two-outlet designs, respectively, while Figure 9d shows the variation in T_{max} among the best-performing designs in the three aforementioned groups. Furthermore, Figure 10a–d shows the temperature contours of the Z-1, best Step-like plenum, best one-outlet, and best two-outlet designs, respectively. The contours show the temperature variation of the cooling air and the batteries in the systems. For instance, in Figure 10a, the inlet section is dominated by cold air, and in its legend, the “blue” color corresponds to the lower-temperature section. However, the most important temperature distributions are those observed among the batteries. Based on the legend's color, it is obvious that the highest temperature in the system was recorded for the batteries, and this was observed for only four batteries. This performance implies that there will be a significant difference in temperature between the first battery and the eighth battery, a phenomenon that indicates poor thermal homogeneity and excess heat accumulation among the four batteries. In order to better understand why Figure 10a shows this poor performance, the distribution of the temperature on the BTMS's contour in Figure 10b is described. In this case, the temperature spreads across the eight batteries, indicating very good thermal homogeneity and the eventual reduction in the maximum temperature,

as shown in the two legends. Similar performance distribution trends are used for other designs, and by comparing the contours in Figure 10 with the results in Figure 9d, it can be seen that the contours provide good insight into the performance of this system. First, in the Step-like plenum category in Figure 9a, where seven different numbers of steps (1, 3, 4, 7, 9, 15, and 19) were investigated, the seven-step design denoted as “Z-2-7” produced the best $T_{max} = 327.78 \text{ K}$, with a reduction by 3.46 K compared with that of the original Z-type design, denoted as “Z-1”, in this study. Designs Z-2-3 (three steps) and Z-2-4 (four steps) also produced good performances, both with reductions in T_{max} by 3.30 K. The poorest of the Step-like plenum designs is Z-2-19 (nineteen steps), which happens to be the only Step-like plenum design that increased T_{max} , with an increase of 0.29 K compared to that of the original Z-type (Z-1) design. For a step design, any modification to another part of the structure, aside from the step, will affect the performance of the BTMS for the same number of steps. Previous studies on the step design have revealed that increasing the number of steps serially does not always result in corresponding increases or decreases in the temperature or pressure drop. However, higher numbers of steps, e.g., 15 and 19, have shown poor performances, which has been reported in previous studies [37,39]. An explanation for this is the fact that the concept of the step design for one and two steps produced poor thermal homogeneity, while for fifteen and nineteen steps, the plenum’s area decreases; hence, the air becomes insufficient to cool down the batteries at that end of the plenum. Figure 9b presents the comparison between the one-outlet designs. From the figure, it can be seen that design Z-5 performed better than the other designs, with a reduction in T_{max} by 1.9 K compared with that of the Z-1 design.

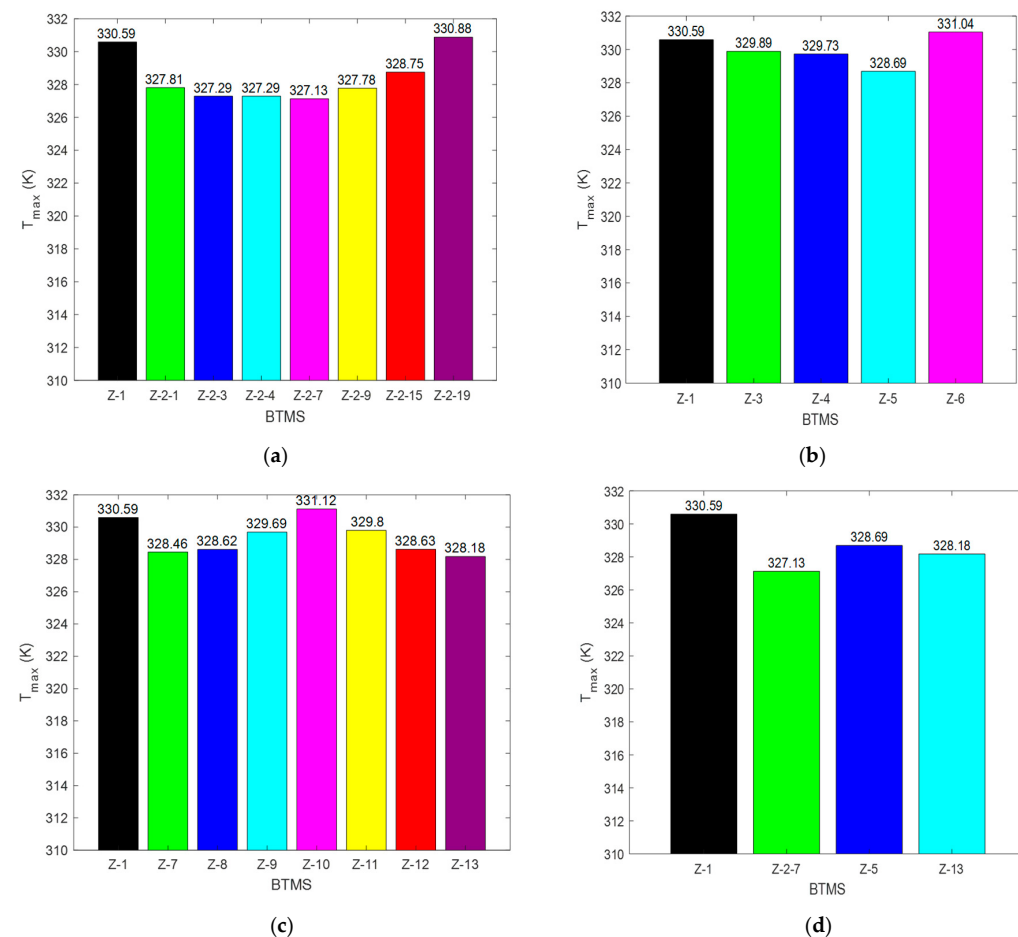


Figure 9. T_{max} performances of BTMSs: (a) Step-like plenum, (b) one outlet, (c) two outlets, and (d) the best in groups (a–c).

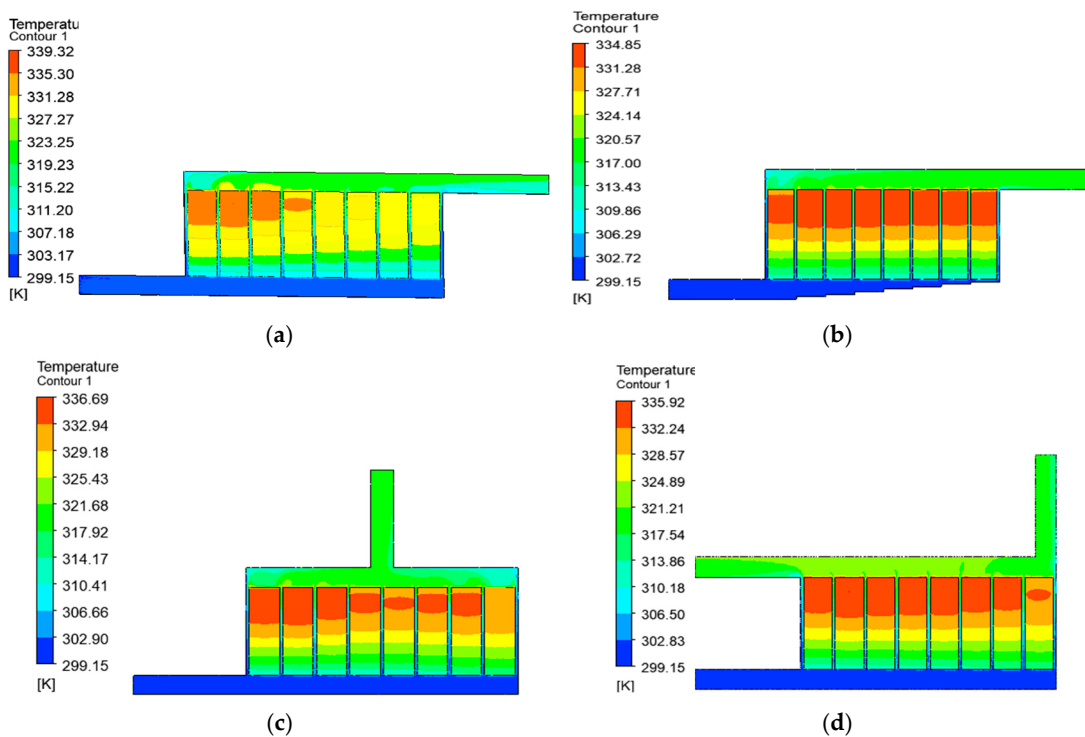


Figure 10. Temperature contours of (a) Z-1, (b) Z-2-7, (c) Z-5, and (d) Z-13 BTMSs.

Furthermore, compared to the Z-1 design, the Z-3 and Z-4 designs also produced better performances, with reductions in T_{max} by 0.7 K and 0.86 K, respectively, while design Z-6 produced a poor performance, with an increase in T_{max} by 0.45 K. Figure 9c presents the comparison of the T_{max} performances for the two-outlet designs. Out of the seven designs considered in this category, only Z-10 (Z-1/Z-6) failed to produce a better performance than that of the Z-1 design, increasing T_{max} by 0.53 K. The other six designs produced reductions in T_{max} , with the Z-13 (Z-3/Z-6) design having the best performance, with a reduction in T_{max} by 2.41 K compared to that of the Z-1 design. The best-performing designs from the three categories were compared and are presented graphically in Figure 9d. From the figure, it can be seen that Z-2-7 produced the best T_{max} performance. Interestingly, in the Z-13 design, a combination of two different outlets (Z-3/Z-6) performed better than the Z-5 design, which happens to be the best-performing design among the one-outlet designs, with a reduction in T_{max} by 0.51 K.

3.1.2. T_{max} Performances of the Combined-Strategy Geometries

The combined-strategy geometries explore the combination of Step-like plenum designs for the considered numbers of steps with the one-outlet designs and two-outlet designs. This implies that each of the four one-outlet designs was investigated when 1, 3, 4, 7, 9, 15, and 19 steps were installed, summing up to twenty-eight designs. Similarly, each of the seven two-outlet designs was investigated for the seven different numbers of steps, summing up to forty-nine designs. These designs were compared, and the best five designs in the two combination groups were selected and are presented in Table 5. Figure 11a,b shows the temperature distribution of the batteries for the combined-strategy geometries with one outlet and two outlets, respectively. The comparison of T_{max} values for the best five performing designs for one outlet and two outlets is presented in Figure 12a,b, respectively. Lastly, the temperature contours of the optimal designs in the one-outlet and two-outlet groups are presented in Figure 13a,b. In Figure 11a,b, the reference Z-type design, denoted as Z-1, is compared with the designs in the two combination groups. The

temperature distribution reveals the temperature uniformity of the best-performing design when compared with those of the reference Z-1 designs.

Table 5. The best five designs of the combined-strategy geometries in terms of T_{max} .

S/N	Step-like Plenum and One-Outlet Combination			Step-like Plenum and Two-Outlet Combination		
	Step	Outlet	T_{max} (K)	Step	Outlet	T_{max} (K)
1.	Z-2-7	Z-6	327.07	Z-2-7	Z-1/Z-6	327.14
2.	Z-2-3	Z-6	327.14	Z-2-3	Z-1/Z-6	327.26
3.	Z-2-4	Z-6	327.63	Z-2-4	Z-1/Z-6	327.59
4.	Z-2-9	Z-6	328.07	Z-2-9	Z-1/Z-6	327.88
5.	Z-2-1	Z-5	328.69	Z-2-7	Z-1/Z-3	328.21

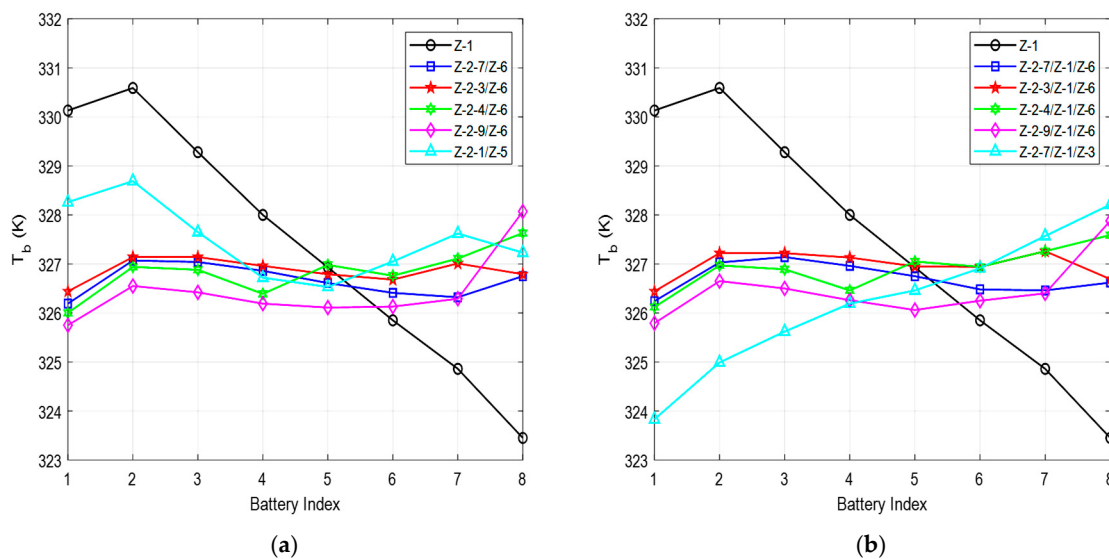


Figure 11. T_b values of combined-strategy designs with (a) one outlet and (b) two outlets.

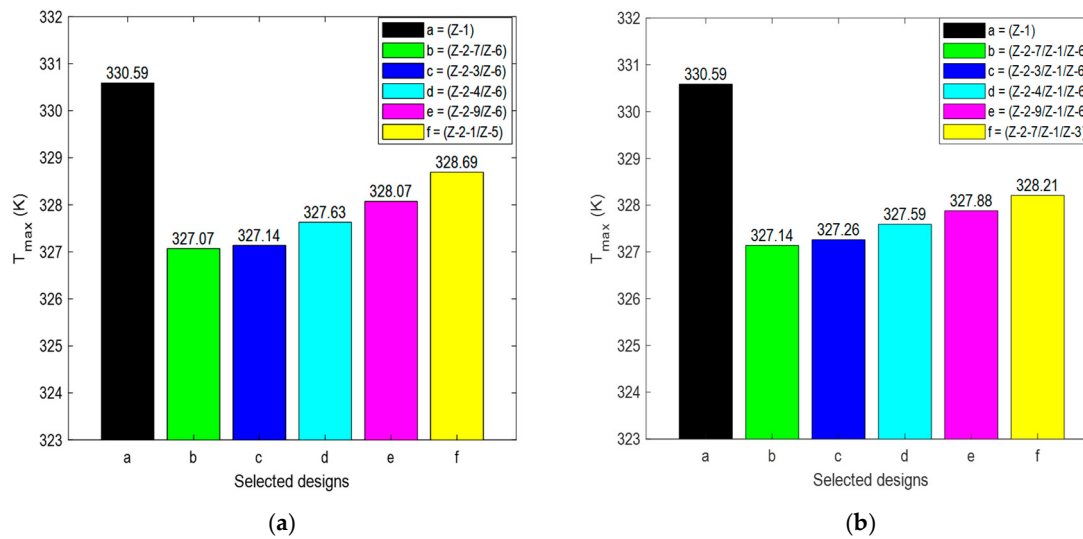


Figure 12. T_{max} values of the batteries for the best five designs with (a) one outlet and (b) two outlets.

Figure 12a,b further presents the comparison between the designs in terms of their T_{max} values. Comparing the one-outlet designs, shown in Figure 12a, the best-performing design is Z-2-7/Z-6, with a minimum T_{max} value of 327.07 K. When compared with the Z-1 designs, it produced a reduction in T_{max} by 3.52 K. Considering the two-outlet designs, presented in Figure 12b, Z-2-7/Z-1/Z-6 produced a minimum T_{max} value of 327.14 K,

and when compared with the reference Z-1 designs, it produced a reduction in T_{max} by 3.45 K. These performances show that both one outlet and two outlets can be combined with a Step-like plenum design to achieve a good reduction in T_{max} . Another intriguing performance shows that Z-2-7/Z-6 also performed better than the initial best Step-like plenum design, which was earlier reported to have performed better than the reference Z-type design without steps. The Z-2-7/Z-6 design reduced the T_{max} of the best reference Step-like plenum design by 0.06 K.

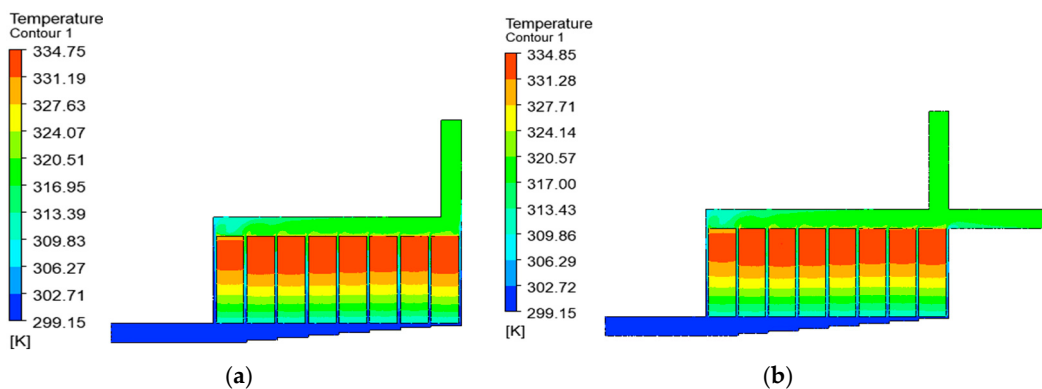


Figure 13. Temperature contours of T_{max} for the best-performing designs with (a) one outlet and (b) two outlets.

3.2. Evaluation of ΔT_{max} Performances

ΔT_{max} is also an important parameter used in evaluating the performance of a BTMS with more than one battery in a pack. This parameter shows the ability of a design to uniformly distribute heat generation in the battery pack, thereby avoiding the overheating of one battery, while the other batteries are at a significantly lower temperature. Such a phenomenon is often regarded as thermal homogeneity. Previous studies in the literature have shown that designs with low ΔT_{max} values produce thermal performances with low T_{max} values. However, one design can produce a lower ΔT_{max} value compared to that of another design under the same operating conditions while still having a higher T_{max} value, although the difference between the ΔT_{max} values may not be significant [28,34,35,44,47]. A better ΔT_{max} value is, however, very important in designs where the cooling air enters the system at extremely low temperatures because any small irregularity of a battery can affect the chemical reaction through a sharp decline in its operating temperature.

3.2.1. ΔT_{max} Performances of Step-like Plenum, One-Outlet, and Two-Outlet Geometries

This subsection focuses on the comparison of the ΔT_{max} values for the Step-like plenum, one-outlet, and two-outlet designs. The optimal designs (with the minimum ΔT_{max} values) in all the design groups are then considered for further comparison. Variations in ΔT_{max} for the Step-like plenum, one outlet, and two outlets, are shown in Figure 14a–c, respectively, while Figure 14d presents the variation of ΔT_{max} between the best-performing designs in the earlier-mentioned groups. In addition, the temperature contours of the Z-1, best Step-like plenum, best one-outlet, and best two-outlet designs are shown in Figure 15a–d, respectively.

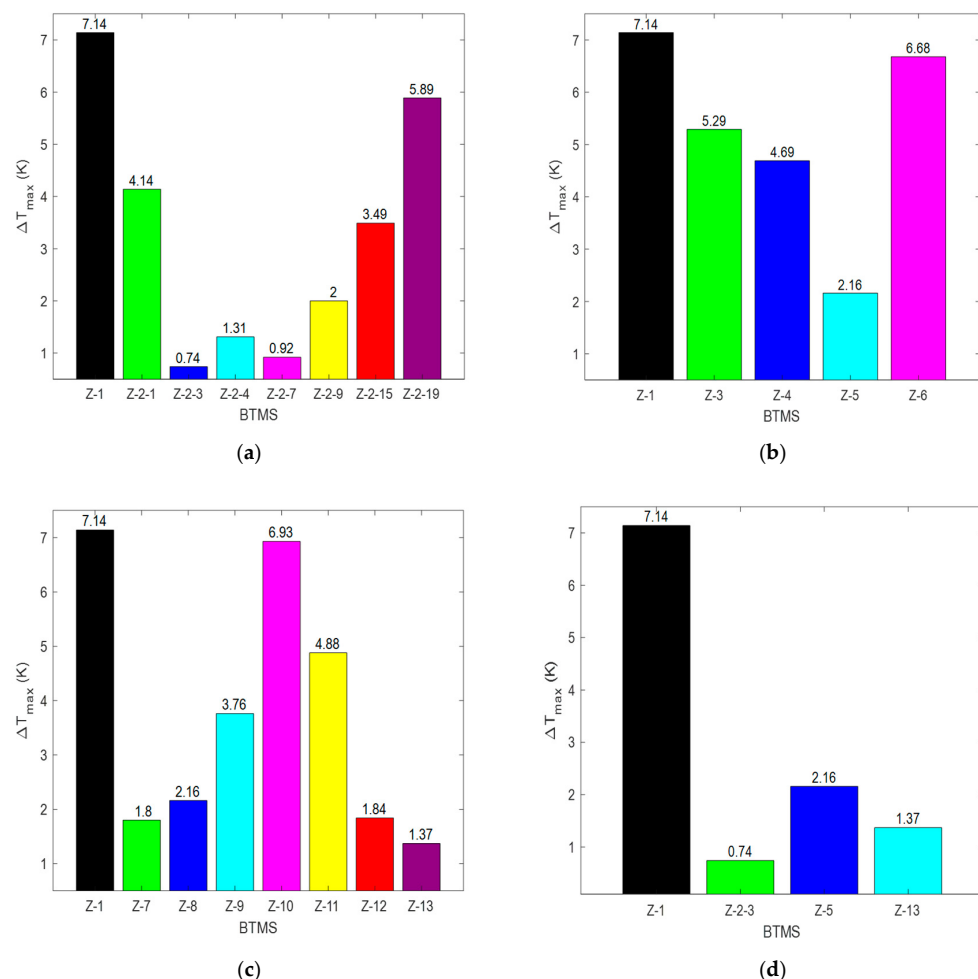


Figure 14. ΔT_{max} performances of BTMSs: (a) Step-like plenum, (b) one outlet, (c) two outlets, and (d) the best in groups (a–c).

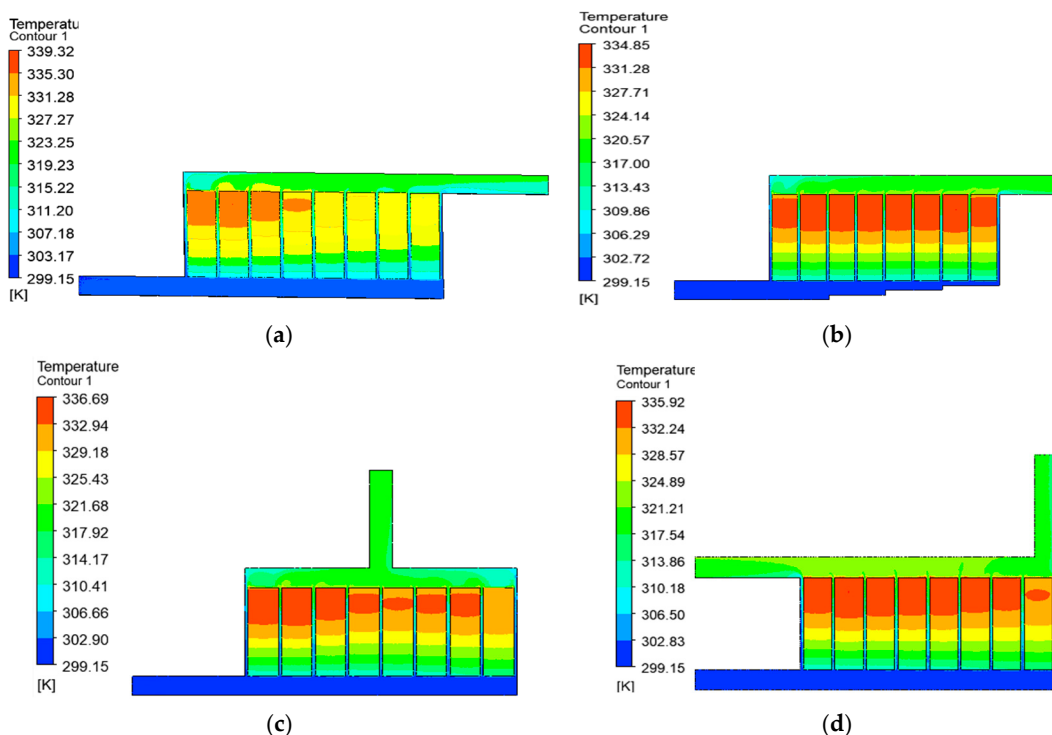


Figure 15. Temperature contours of (a) Z-1, (b) Z-2-3, (c) Z-5, and (d) Z-13 BTMSs.

For the Step-like plenum designs in Figure 14a, the three-step design, denoted as “Z-2-3”, produced the best ΔT_{max} performance, with a recorded value of 0.74 K. When compared with the ΔT_{max} value of the Z-1 design, the ΔT_{max} value of Z-2-3 reduced by 6.4 K. In general, as shown in Figure 14a, every Step-like plenum design produced a good ΔT_{max} performance, with Z-2-4 (four steps) and Z-2-7 (seven steps) producing reductions by 5.84 K and 6.22 K, respectively, compared with that of the Z-1 design. Figure 14b shows the performances of the one-outlet designs. Design Z-5 has the minimum ΔT_{max} value, recorded at 2.16 K, and compared with the ΔT_{max} value of the reference Z-1 design, produced a reduction by 4.98 K. The remaining one-outlet flow designs also produced ΔT_{max} reductions by 2.45 K, 1.85 K, and 0.46 K for Z-3, Z-4, and Z-6, respectively. Figure 14c shows the performance comparison of the two-outlet designs. The results revealed that design Z-10 produced the poorest performance, while design Z-13 produced the best, with ΔT_{max} values of 6.93 K and 1.37 K, respectively, and reductions by 0.21 K and 5.77 K, respectively, compared with that of the reference Z-1 design. The best-performing designs selected from Figure 14a–c were also compared and are presented in Figure 14d. The results revealed that design Z-2-3 has the best performance, with a ΔT_{max} value of 0.74 K, and when compared with the performances of the Z-5 and Z-13 designs, produced reductions by 1.42 K and 0.63 K, respectively.

3.2.2. ΔT_{max} Performances of the Combined-Strategy Geometries

The ΔT_{max} performances in this section also consider the same geometries for comparison as those in the case of T_{max} . The designs were compared, and the best five in the two groups of combinations are presented in Table 6. Figure 16a,b shows the comparison of the best-performing designs in terms of ΔT_{max} for the one-outlet and two-outlet designs, respectively. Additionally, the temperature contours of the best-performing designs in the one-outlet and two-outlet groups are presented in Figure 17a,b. Figure 16a,b presents the comparison of the reference Z-1 designs with the designs in the two combination groups.

Table 6. The best five designs of combined-strategy geometries in terms of ΔT_{max} .

S/N	Step-like Plenum and One-Outlet Combination			Step-like Plenum and Two-Outlet Combination		
	Step	Outlet	ΔT_{max} (K)	Step	Outlet	ΔT_{max} (K)
1.	Z-2-3	Z-6	0.70	Z-2-3	Z-1/Z-6	0.82
2.	Z-2-7	Z-6	0.88	Z-2-7	Z-1/Z-6	0.90
3.	Z-2-4	Z-6	1.63	Z-2-4	Z-1/Z-6	1.47
4.	Z-2-1	Z-5	2.16	Z-2-1	Z-1/Z-5	1.94
5.	Z-2-9	Z-6	2.32	Z-2-9	Z-1/Z-6	2.09

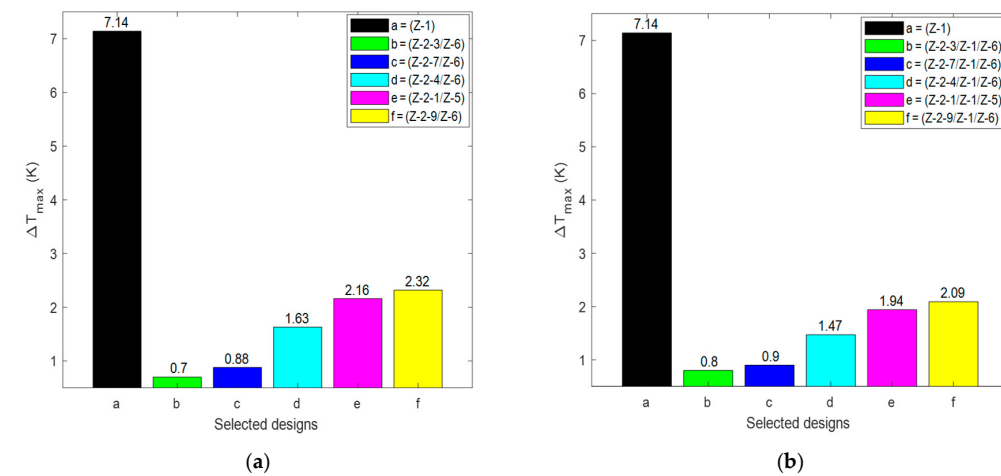


Figure 16. ΔT_{max} values of the batteries for the best five designs with (a) one outlet and (b) two outlets.

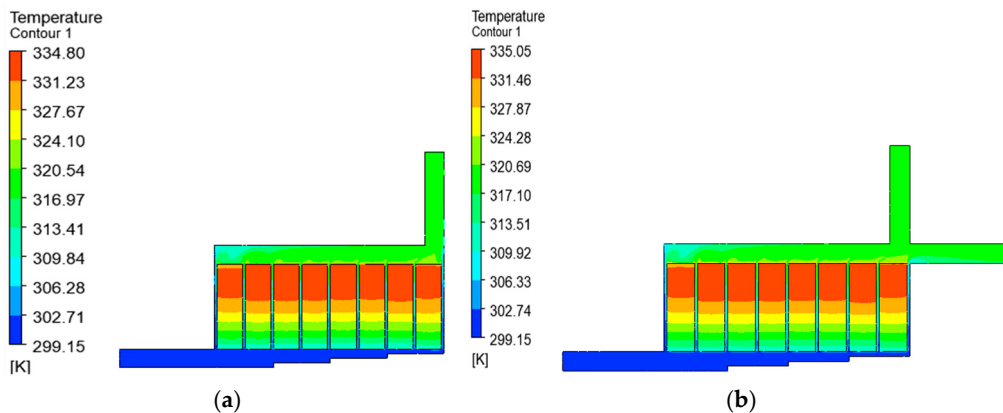


Figure 17. Temperature contours of ΔT_{max} for the best-performing designs with (a) one outlet and (b) two outlets.

Comparing the one-outlet designs presented in Figure 16a, design Z-2-3/Z-6 produced the best performance, with a ΔT_{max} value of 0.7 K, while the poorest was produced by design Z-2-9/Z-6, with a ΔT_{max} value of 2.32 K. Both the best- and poorest-performing designs performed significantly better than the reference Z-1 design, with reductions by 6.44 K and 4.82 K, respectively. In Figure 16b, the performances of the best five two-outlet designs show that these five designs also performed significantly better than the reference Z-1 design. Furthermore, the Z-2-3/Z-1/Z-6 design produced the best performance, while design Z-2-9/Z-1/Z-6 produced the poorest. Additionally, it was observed that the ΔT_{max} values were reduced by 6.34 K and 5.05 K, when compared with those of Z-2-3/Z-1/Z-6 and Z-2-9/Z-1/Z-6, respectively.

3.3. Evaluation of ΔP Performances

In air-cooled BTMSs, especially where external devices are used to pump the cooling air, it is necessary to take into consideration the pumping cost, which is related to the pressure drop. Previous studies have shown that the structural redesign of BTMSs and increases in the cooling air's velocity can minimize both T_{max} and ΔT_{max} . However, this comes with the drawback of an increase in ΔP . With continuous research in the redesign of BTMSs, both T_{max} and ΔT_{max} are being enhanced, with minimal ΔP increases and without the need to increase the air's velocity.

3.3.1. ΔP Performances of the Step-like Plenum, One-Outlet, and Two-Outlet Geometries

This section considered the ΔP performances of the designs with Step-like plenums, one outlet, and two outlets for comparison. The best-performing designs (with the minimum ΔP values) in each group were then compared. Figure 18a–c presents the variations in ΔP for the Step-like plenum, one-outlet, and two-outlet designs, respectively, while Figure 18d shows the variation in ΔP between the best-performing designs in each of the three groups. Lastly, Figure 19a–d shows the pressure contours of the Z-1, best Step-like plenum, best one-outlet, and best two-outlet designs, respectively.

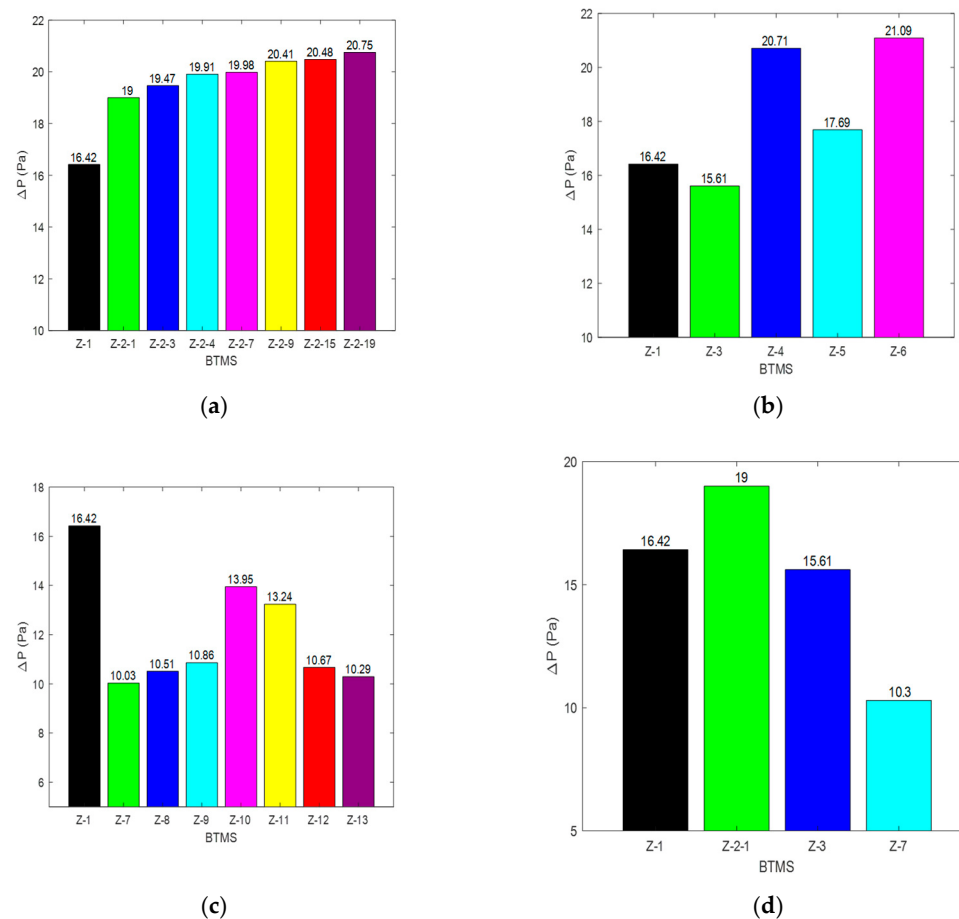


Figure 18. ΔP performances of BTMSs: (a) Step-like plenum, (b) one outlet, (c) two outlets, and (d) the best in groups (a–c).

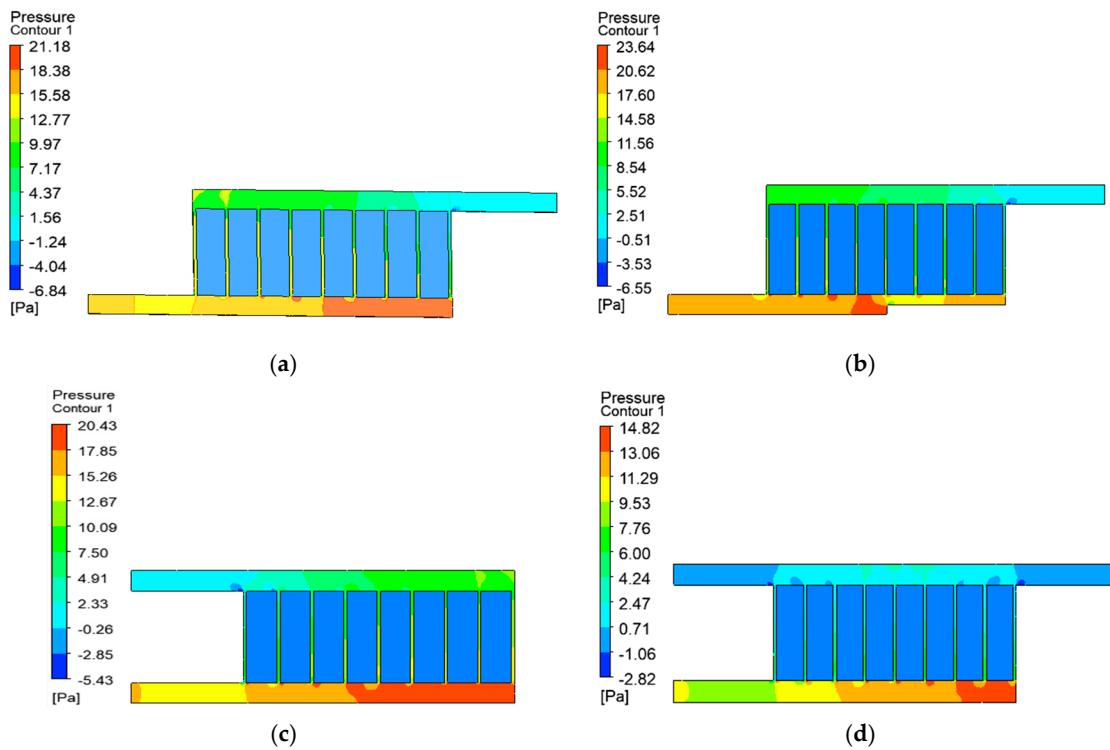


Figure 19. Temperature contours of (a) Z-1, (b) Z-2-1, (c) Z-3, and (d) Z-7 BTMSs.

The Step-like plenum designs are first considered and presented in Figure 18a. From the figure, it can be seen that the Z-1 design performed better than all the other designs, while the Z-2-1 design produced the minimum ΔP value among the Step-like plenum designs. The ΔP performances of the Step-like plenum designs also show increases in ΔP with increases in the number of steps. Z-2-1, being the best-performing design, produced an increase in ΔP by 2.58 Pa, when compared with that of the Z-1 design. The poorest performance was observed for design Z-2-19, which produced an increase in ΔP by 4.33 Pa. Next, are the performances of the one-outlet designs presented in Figure 18b. The results reveal that design Z-3 produced the best performance, with a reduction in ΔP by 0.81 Pa when compared with that of the reference Z-1 design. However, the remaining one-outlet designs did not perform better than the Z-1 design, recording increases in ΔP by 4.29 Pa, 1.27 Pa, and 4.67 Pa for Z-4, Z-5, and Z-6, respectively. The performances of the two-outlet designs were also considered and are presented in Figure 18c. First, the performances show that all the two-outlet designs produced lower ΔP values compared with that of the reference Z-1 design. Second, Z-7 produced the minimum value, and compared with the Z-1 design, yielded a reduction in ΔP by 6.39 Pa. Figure 18d further presents the performances of the best-performing designs in each of the three groups, and design Z-7 clearly produced the best performance.

3.3.2. ΔP Performances of the Combined-Strategy Geometries

This section explores the performances of the combined-strategy designs with respect to ΔP . The designs were compared, and the best five in the two groups of combinations are presented in Table 7. Figure 20a,b shows the comparison of the best-performing designs in terms of ΔP for one outlet and two outlets, respectively. Additionally, the pressure contours of the best-performing designs with one outlet and two outlets are presented in Figure 21a,b. Figure 20a presents the comparison among the one-outlet designs. From the figure, the Z-1 design performed better than all the best five one-outlet designs. When focusing on the one-outlet combinations only, design Z-2-1/Z-3 produced the best performance, with a ΔP value of 17.13 Pa, while the poorest-performing design, Z-2-4/Z-3, produced a ΔP value of 18.71 Pa. Figure 20b further presents the performances of the two-outlet designs. From the figure, all the five best-performing designs performed better than the Z-1 design. Among the two-outlet designs, Z-2-1/Z-1/Z-4 and Z-2-1/Z-1/Z-5 produced the best and poorest performances, respectively, reducing ΔP by 5.91 Pa and 3.66 Pa, respectively, when compared with the ΔP value of the reference Z-1 design.

Table 7. The best five designs of the combined-strategy geometries in terms of ΔP .

S/N	Step-like Plenum and One-Outlet Combination			Step-like Plenum and Two-Outlet Combination		
	Step	Outlet	ΔP (Pa)	Step	Outlet	ΔP (Pa)
1.	Z-2-1	Z-3	17.13	Z-2-1	Z-1/Z-4	10.51
2.	Z-2-1	Z-5	17.69	Z-2-1	Z-1/Z-3	11.67
3.	Z-2-3	Z-3	18.27	Z-2-1	Z-3/Z-6	11.97
4.	Z-2-7	Z-3	18.68	Z-2-1	Z-3/Z-5	12.03
5.	Z-2-4	Z-3	18.71	Z-2-1	Z-1/Z-5	12.76

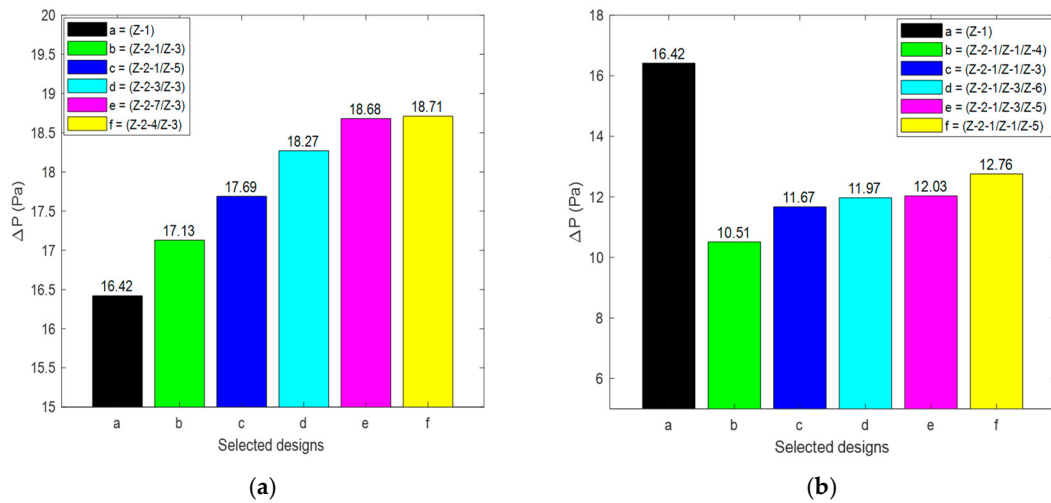


Figure 20. ΔP values of the batteries for the best five designs with (a) one outlet and (b) two outlets.

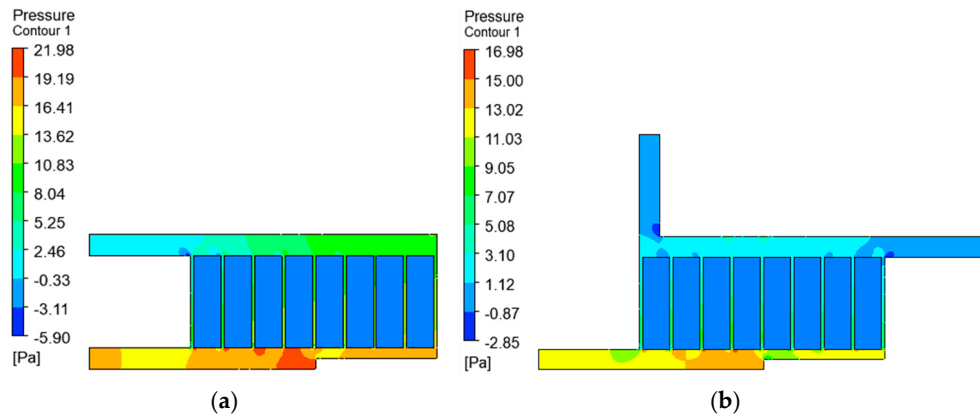


Figure 21. Pressure contours of ΔP for the best-performing designs with (a) one outlet and (b) two outlets.

4. Conclusions

The redesign of the Z-type BTMS has brought about a drop in T_{max} , though with a significant increase in ΔP , hence requiring studies to focus on means of decreasing the pressure drop by exploring new designs. In this study, the Step-like plenum design was further investigated by observing the effects of two outlets on the performances of the systems with the aim of reducing or maintaining T_{max} and minimizing ΔP . The CFD approach was used to compute the performances of the designs. The designs explore combinations of Step-like plenum designs having different numbers of steps (N_s) = 1, 3, 4, 7, 9, 15, and 19 with one and two air outlets. From the results obtained, the following conclusions were drawn:

1. The initial Step-like plenum design with seven steps (Z-2-7) produced the best T_{max} (327.13 K) among the Step-like plenum categories of the reference Z-type BTMSs, with a reduction by 3.46 K compared to that of the original Z-type design without any steps installed. For the one-outlet designs, the best-performing design is Z-2-7/Z-6, with a minimum T_{max} value of 327.07 K, and compared with the original Z-type designs, it produced a reduction in T_{max} by 3.52 K. For the two-outlet designs, design Z-2-7/Z-1/Z-6 produced a minimum T_{max} value of 327.14 K, and when compared to the original Z-1 designs, it produced a reduction in T_{max} by 3.45 K. The Z-2-7/Z-6 design reduced the T_{max} value of the best Step-like plenum design by 0.06 K;
2. By comparing the Step-like plenum, one-outlet, and two-outlet designs, the Z-2-3 design has the best performance, with a ΔT_{max} value of 0.74 K, and compared with

the Z-5 and Z-13 designs, it produced reductions in ΔT_{max} by 1.42 K and 0.63 K, respectively. Considering the best five two-outlet designs, with respect to the ΔT_{max} performance, significant performance improvements were observed when compared with that of the reference Z-type design. The Z-2-3/Z-1/Z-6 design produced the best performance, while design Z-2-9/Z-1/Z-6 produced the poorest. It was observed that the ΔT_{max} value reduced by 6.34 K and 5.05 K when compared with those of Z-2-3/Z-1/Z-6 and Z-2-9/Z-1/Z-6, respectively;

3. For the designs in the three groups, Z-7 produced the minimum value, and compared with the Z-1 design, it yielded a reduction in ΔP by 6.39 Pa. In terms of ΔP , the Step-like plenum and one-outlet combination designs produced good performances. The Z-2-1/Z-3 design produced the best performance, with a ΔP value of 17.13 Pa, while the poorest-performing design, Z-2-4/Z-3, produced a ΔP value of 18.71 Pa. Among the best five two-outlet designs with and without a Step-like plenum structure, Z-2-1/Z-1/Z-4 and Z-2-1/Z-1/Z-5 produced the best and poorest performances, reducing ΔP by 5.91 Pa and 3.66 Pa, respectively.

Author Contributions: Conceptualization, O.M.O.; Methodology, O.M.O., E.T.I., M.J.L., M.C.H. and M.L.D.; Software, O.M.O., E.T.I., M.J.L., M.C.H. and M.L.D.; Validation, O.M.O., E.T.I., M.J.L., M.C.H. and M.L.D.; Formal analysis, O.M.O., E.T.I., M.J.L., M.C.H. and M.L.D.; Investigation, O.M.O., E.T.I., M.J.L., M.C.H. and M.L.D.; Resources, O.M.O.; Data curation, O.M.O.; Writing—original draft, O.M.O., E.T.I., M.J.L., M.C.H. and M.L.D.; Writing—review & editing, O.M.O., E.T.I., M.J.L., M.C.H. and M.L.D.; Visualization, O.M.O.; Supervision, O.M.O.; Project administration, O.M.O. All authors have read and agreed to the published version of the manuscript.

Funding: This research received no external funding.

Data Availability Statement: The original contributions presented in the study are included in the article, further inquiries can be directed to the corresponding author.

Conflicts of Interest: The authors declare no conflict of interest.

Nomenclature

Acronym		Unit
SOC	State of charge	-
TMS	Thermal management system	-
BTMS	Battery thermal management system	-
CFD	Computational fluid dynamics	-
HTMS	Hybrid thermal management system	-
PCM	Phase-change material	-
EV	Electric vehicle	-
Symbol(s)		
L_s	Step length	mm
H_s	Step height	mm
L_{ns}	Non-stepped length	mm
L_{ts}	Stepped length	mm
L_{ins}	Initial non-stepped length	mm
P_i and P_o	Average pressures of cooling air at the inlet and outlet(s)	Pa
T_{max}	The maximum temperature of the batteries	K
T_{min}	The minimum temperature of the batteries	K
ΔT_{max}	The maximum temperature difference of the batteries	K
ΔP	Pressure drop	Pa

A_i	Inlet sections' cross-sectional area	m^2
\dot{V}	Volume flow rate of the air	m^3/s
u_i	Velocity vector's i th component	-
x, y , and z	x -, y -, and z -coordinates, respectively	-
Re	Reynolds number	-
T_b	Temperature of the battery	K
I	Discharge current	A
R_b	Battery's equivalent resistance	Ω
Q_b	Battery's heat generation rate	W/m^3
V_b	Volume of the battery	m^3
k_a	Thermal conductivity (air)	$\text{W}/\text{m.K}$
k_b	Thermal conductivity (battery)	$\text{W}/\text{m.K}$
c_a	Specific heat capacity (air)	$\text{J}/\text{kg.K}$
c_b	Specific heat capacity (battery)	$\text{J}/\text{kg.K}$
D_h	Inlet's hydraulic diameter	mm
G_k and G_b	Average velocity gradients and buoyancy effects, respectively, for turbulence kinetic energy generation	-
Υ_M	Contribution of the fluctuating dilatation in compressible turbulence to the overall dissipation rate	-
$C_{1\varepsilon}, C_{2\varepsilon}, C_{3\varepsilon}$	Model constants	-
S_k and S_ε	Source terms	-
Greek letter(s)		
ρ_a	Density (air)	kg/m^3
ρ_b	Density (battery)	kg/m^3
μ_a	Dynamic viscosity (air)	$\text{kg}/\text{m.s}$
μ_t	Turbulent dynamic viscosity	$\text{kg}/\text{m.s}$
σ_k and σ_ε	k - and ε -turbulences' Prandtl numbers	-

References

- Mo, C.; Xie, J.; Zhang, G.; Zou, Z.; Yang, X. All-climate battery thermal management system integrating units-assembled phase change material module with forced air convection. *Energy* **2024**, *294*, 130642. [[CrossRef](#)]
- Na, X.; Kang, H.; Wang, T.; Wang, Y. Reverse layered air flow for Li-ion battery thermal management. *Appl. Therm. Eng.* **2018**, *143*, 257–262. [[CrossRef](#)]
- Zhong, G.; Zhang, G.; Yang, X.; Li, X.; Wang, Z.; Yang, C.; Yang, C.; Gao, G. Researches of composite phase change material cooling/resistance wire preheating coupling system of a designed 18650-type battery module. *Appl. Therm. Eng.* **2017**, *127*, 176–183. [[CrossRef](#)]
- Dan, D.; Yao, C.; Zhang, H.; Zeng, Z.; Xu, X. Dynamic thermal behavior of micro heat pipe array-air cooling battery thermal management system based on thermal network model. *Appl. Therm. Eng.* **2019**, *162*, 114183. [[CrossRef](#)]
- Rao, Z.; Wang, S. A review of power battery thermal energy management. *Renew. Sustain. Energy Rev.* **2011**, *15*, 4554–4571. [[CrossRef](#)]
- Yong, S.C.; Mo, K.D. Prediction of thermal behaviors of an air-cooled lithium-ion battery system for hybrid electric vehicles. *J. Power Sources* **2014**, *270*, 273–280. [[CrossRef](#)]
- Mohammadian, S.K.; Zhang, Y. Thermal management optimization of an air-cooled Li-ion battery module using pin fin heat sinks for hybrid electric vehicles. *J. Power Sources* **2015**, *273*, 431–439. [[CrossRef](#)]
- Yang, X.; Tan, S.; Liu, J. Thermal management of li-ion battery with liquid metal. *Energy Convers. Manag.* **2016**, *117*, 577–585. [[CrossRef](#)]
- Wang, C.; Zhang, G.; Meng, L.; Li, X.; Situ, W.; Lv, Y.; Rao, M. Liquid cooling based on thermal silica plate for battery thermal management system. *Int. J. Energy Res.* **2017**, *41*, 2468–2479. [[CrossRef](#)]
- Liang, J.; Gan, Y.; Li, Y. Investigation on the thermal performance of a battery thermal management system using heat pipe under different ambient temperatures. *Energy Convers. Manag.* **2018**, *155*, 1–9. [[CrossRef](#)]
- Liang, Z.; Wang, R.; Malt, A.H.; Souri, M.; Esfahani, M.; Jabbari, M. Systematic evaluation of a flat-heat-pipe-based thermal management: Cell-to-cell variations and battery ageing. *Appl. Therm. Eng.* **2021**, *192*, 116934. [[CrossRef](#)]

12. Rao, Z.; Wang, Q.; Huang, C. Investigation of the thermal performance of phase change material/mini-channel coupled battery thermal management system. *Appl. Energy* **2016**, *164*, 659–669. [\[CrossRef\]](#)
13. Samimi, F.; Babapoor, A.; Azizi, M.; Karimi, G. Thermal management analysis of a li-ion battery cell using phase change material loaded with carbon fibers. *Energy* **2016**, *96*, 355–371. [\[CrossRef\]](#)
14. Zhao, Y.; Li, Q.; Zou, B.; Zhang, T.; Jin, L.; Qiao, G.; Nie, B.; Huang, Y.; Ding, Y. Performance of a liquid cooling-based battery thermal management system with a composite phase change material. *Int. J. Energy Res.* **2020**, *44*, 4727–4742. [\[CrossRef\]](#)
15. Mashayekhi, M.; Houshfar, E.; Ashjaee, M. Development of hybrid cooling method with PCM and Al₂O₃ nanofluid in aluminium minichannels using heat source model of Li-ion batteries. *Appl. Therm. Eng.* **2020**, *178*, 115543. [\[CrossRef\]](#)
16. El Idi, M.M.; Karkri, M.; Tankari, M.A.; Vincent, S. Hybrid cooling based battery thermal management using composite phase change materials and forced convection. *J. Energy Storage* **2021**, *41*, 102946. [\[CrossRef\]](#)
17. Li, Y.; Kong, B.; Qiu, C.; Li, Y.; Jiang, Y. Numerical study on air-cooled battery thermal management system considering the sheer altitude effect. *Appl. Therm. Eng.* **2025**, *258*, 124707. [\[CrossRef\]](#)
18. Fan, Y.; Zuo, X.; Zhan, D.; Zhao, J.; Zhang, G.; Wang, H.; Wang, K.; Yang, S.; Tan, X. A novel control strategy for active battery thermal management systems based on dynamic programming and a genetic algorithm. *Appl. Therm. Eng.* **2023**, *233*, 121113. [\[CrossRef\]](#)
19. Qin, P.; Liao, M.; Zhang, D.; Liu, Y.; Sun, J.; Wang, Q. Experimental and numerical study on a novel hybrid battery thermal management system integrated forced-air convection and phase change material. *Energy Convers. Manag.* **2019**, *195*, 1371–1381. [\[CrossRef\]](#)
20. Behi, H.; Karimi, D.; Behi, M.; Ghanbarpour, M.; Jaguemont, J.; Sokkeh, M.A.; Gandoman, F.H.; Berecibar, M.; Mierlo, J.V. A new concept of thermal management system in Li ion battery using air cooling and heat pipe for electric vehicles. *Appl. Therm. Eng.* **2020**, *174*, 115280. [\[CrossRef\]](#)
21. Zhang, N.; Zhang, Z.; Li, J.; Cao, X. Performance analysis and prediction of hybrid battery thermal management system integrating PCM with air cooling based on machine learning algorithm. *Appl. Therm. Eng.* **2024**, *257*, 124474. [\[CrossRef\]](#)
22. Zhou, L.; Li, S.; Jain, A.; Chen, G.; Guo, D.; Kang, J.; Zhao, Y. Lithium Battery Thermal Management Based on Liightweight Stepped-Channel Liquid Cooling. *ASME J. Electrochem. Energy Convers. Storage* **2024**, *21*, 031012-1. [\[CrossRef\]](#)
23. Song, K.; He, R.; Gao, C.; Pea, H.J.M.; He, A.; Zhang, Q.; Zhang, K.; An, Z. Performance of a combined battery thermal management system with dual-layer phase change materials and air cooling technologies. *Appl. Therm. Eng.* **2024**, *254*, 123865. [\[CrossRef\]](#)
24. Zhu, X.; Liao, X.; Kang, S.; Sun, L.; Zhao, Y. Optimization design of lithium battery management system based on Z-F composite air cooling structure. *J. Energy Storage* **2024**, *102 Pt A*, 114068. [\[CrossRef\]](#)
25. Lamba, R.; Montero, F.J.; Rehman, T.; Singh, S.; Manikandan, S. PCM-based hybrid thermal management system for photovoltaic modules: A comparative analysis. *Environ. Sci. Pollut. Res.* **2024**, *31*, 46397–46416. [\[CrossRef\]](#) [\[PubMed\]](#)
26. Moaveni, A.; Siavashi, M.; Mousavi, S. Passive and hybrid battery thermal management system by cooling flow control, employing nano-PCM, fins, and metal foam. *Energy* **2024**, *288*, 129809. [\[CrossRef\]](#)
27. Argade, S.; De, A. Optimization study of a Z-type airflow cooling system of a lithium-ion battery pack. *Phys. Fluids* **2024**, *36*, 067119. [\[CrossRef\]](#)
28. Oyewola, O.M.; Idowu, E.T. Wave and straight plenum effects on thermal management system performance. *Int. J. Thermofluids* **2024**, *22*, 100678. [\[CrossRef\]](#)
29. Suo, Y.; Tang, C.; Han, E.; Chen, Z. Comparative assessment and optimization among several plenum shapes and positions for the forced air-cooled battery thermal management system. *J. Energy Storage* **2024**, *99 Pt B*, 113319. [\[CrossRef\]](#)
30. Chen, K.; Zhang, Z.; Wu, B.; Song, M.; Wu, X. An air-cooled system with a control strategy for efficient battery thermal management. *Appl. Therm. Eng.* **2024**, *236 Pt B*, 121578. [\[CrossRef\]](#)
31. Alzwayi, A.; Paul, M.C. Effective battery pack cooling by controlling flow patterns with vertical and spiral fins. *Therm. Sci. Eng. Prog.* **2024**, *55*, 102907. [\[CrossRef\]](#)
32. Qin, P.; Liao, M.; Mei, W.; Sun, J.; Wang, Q. The experimental and numerical investigation on a hybrid battery thermal management system based on forced-air convection and internal finned structure. *Appl. Therm. Eng.* **2021**, *195*, 117212. [\[CrossRef\]](#)
33. Wang, N.; Li, C.; Huang, M.; Qi, D. Effect analysis on performance enhancement of a novel air cooling battery thermal management system with spoilers. *Appl. Therm. Eng.* **2021**, *192*, 116932. [\[CrossRef\]](#)
34. Wang, M.; Hung, C.; Xi, H. Numerical Study on Performance Enhancement of the Air Cooled Battery Thermal Management System by Adding Parallel Plates. *Energies* **2021**, *14*, 3096. [\[CrossRef\]](#)
35. Oyewola, O.M.; Idowu, E.T.; Drabo, M.L. Influence of straight and inclined baffles on enhancement of battery thermal management system performance. *Heliyon* **2024**, *10*, e38585. [\[CrossRef\]](#) [\[PubMed\]](#)
36. Alzwayi, A.; Paul, M.C. Heat transfer enhancement of a lithium-ion battery cell using vertical and spiral cooling fins. *Therm. Sci. Eng. Prog.* **2024**, *47*, 102304. [\[CrossRef\]](#)

37. Oyewola, O.M.; Awonusi, A.A.; Ismail, O.S. Design optimization of Air-Cooled Li-ion battery thermal management system with Step-like divergence plenum for electric vehicles. *Alex. Eng. J.* **2023**, *71*, 631–644. [[CrossRef](#)]
38. Oyewola, O.M.; Awonusi, A.A.; Ismail, O.S. Performance Optimization of Step-like Divergence Plenum Air-Cooled Li-Ion Battery Thermal Management System Using Variable-Step-Height Configuration. *Emerg. Sci. J.* **2024**, *8*, 795–814. [[CrossRef](#)]
39. Oyewola, O.M.; Idowu, E.T. Numerical and artificial neural network inspired study on Step-like-plenum battery thermal management system. *Int. J. Thermofluids* **2024**, *24*, 100897. [[CrossRef](#)]
40. Chen, K.; Wu, W.; Yuan, F.; Chen, L.; Wang, S. Cooling efficiency improvement of air-cooled battery thermal management system through designing the flow pattern. *Energies* **2019**, *167*, 781–790. [[CrossRef](#)]
41. Chen, K.; Hou, J.; Wu, X.; Chen, Y.; Song, M.; Wang, S. Design of flow pattern in air-cooled battery thermal management system. *Int. J. Energy Res.* **2021**, *45*, 9541–9554. [[CrossRef](#)]
42. Wang, C.; Xi, H.; Wang, M. Investigation of forced air-cooling strategy of battery thermal management system considering the inconsistency of battery cells. *Appl. Therm. Eng.* **2022**, *214*, 118841. [[CrossRef](#)]
43. Hong, S.; Zhang, X.; Chen, K.; Wang, S. Design of flow configuration for parallel air-cooled battery thermal management system with secondary vent. *Int. J. Heat Mass Transf.* **2018**, *116*, 1204–1212. [[CrossRef](#)]
44. Oyewola, O.M.; Idowu, E.T. Effects of Step-like plenum, flow pattern and inlet flow regime on thermal management system. *Appl. Therm. Eng.* **2024**, *243*, 122637. [[CrossRef](#)]
45. Yan, H.; Ma, X.; Chen, Y.; Tao, Q.; Song, M. Performance analysis of a wet pad assisted air cooled battery thermal management system with varying number of battery cells. *Appl. Therm. Eng.* **2024**, *259*, 124747. [[CrossRef](#)]
46. Zhang, F.; Lin, A.; Wang, P.; Liu, P. Optimization design of a parallel air-cooled battery thermal management system with spoilers. *Appl. Therm. Eng.* **2021**, *182*, 116062. [[CrossRef](#)]
47. Wang, M.; Teng, S.; Xi, H.; Li, Y. Cooling performance optimization of air-cooled battery thermal management system. *Appl. Therm. Eng.* **2021**, *195*, 117242. [[CrossRef](#)]

Disclaimer/Publisher’s Note: The statements, opinions and data contained in all publications are solely those of the individual author(s) and contributor(s) and not of MDPI and/or the editor(s). MDPI and/or the editor(s) disclaim responsibility for any injury to people or property resulting from any ideas, methods, instructions or products referred to in the content.